Effects of Terminal Dimethylation and Metal Coordination of Proline-2-Formylpyridine Thiosemicarbazone Hybrids on Lipophilicity, Anti-proliferative Activity and hR2 RNR inhibition

Felix Bacher,[#] Orsolya Dömötör,[†] Maria Kaltenbrunner,[#] Miloš Mojović,[§] Ana Popović-Bijelić,[§] Astrid Gräslund,[Δ] Andrew Ozarowski,[∀] Lana Filipovic,[▽] Sinisa Radulović,[▽] Éva A. Enyedy,*[,‡] Vladimir B. Arion*[,#]

[#]*University of Vienna, Faculty of Chemistry, Institute of Inorganic Chemistry, Währinger Strasse 42, A-1090 Vienna, Austria,* [†]*MTA-SZTE Bioinorganic Chemistry Research Group, University of Szeged, Dóm tér 7, H-6720 Szeged, Hungary,* [§]*Faculty of Physical Chemistry, University of Belgrade, Serbia,* [Δ]*Department of Biochemistry and Biophysics, Stockholm University, S-10691 Stockholm, Sweden,* [∀]*National High Magnetic Field Laboratory, Florida State University, Tallahassee, FL32310, USA,* [▽]*Institute for Oncology and Radiology of Serbia, Pasterova 14, 11000 Belgrade, Serbia,* [‡]*Department of Inorganic and Analytical Chemistry, University of Szeged, Dóm tér 7. H-6720 Szeged, Hungary*

Keywords: Proline-thiosemicarbazone hybrids, Solution equilibrium, Stability constants, Antitumor activity, hR2 RNR

Abstract

The nickel(II), copper(II) and zinc(II) complexes of the proline-thiosemicarbazone hybrids 3-methyl-(*S*)-pyrrolidine-2-carboxylate-2-formylpyridine thiosemicarbazone (L-Pro-FTSC or (*S*)-H_2L^1) and 3-methyl-(*R*)-pyrrolidine-2-carboxylate-2-formylpyridine thiosemicarbazone (D-Pro-FTSC or (*R*)-H_2L^1), as well as 3-methyl-(*S*)-pyrrolidine-2-carboxylate-2-formylpyridine 4,4-dimethyl-thiosemicarbazone (dm-L-Pro-FTSC or (*S*)-H_2L^2), namely [Ni(L-Pro-FTSC−2H)]$_2$ (**1**), [Ni(D-Pro-FTSC−2H)]$_2$ (**2**), [Ni(dm-L-Pro-FTSC−2H)]$_2$ (**3**), [Cu(dm-L-Pro-FTSC−2H)] (**6**), [Zn(L-Pro-FTSC−2H)] (**7**) and [Zn(D-Pro-FTSC−2H)] (**8**), in addition to two previously reported, [Cu(L-Pro-FTSC−2H)] (**4**), [Cu(D-Pro-FTSC−2H)] (**5**), have been synthesized and characterized by elemental analysis, one- and two-dimensional ^{1}H and ^{13}C NMR spectroscopy, CD, UV−vis and ESI mass spectrometry. Compounds **1–3**, **6** and **7** have been also studied by single crystal X-ray diffraction. Magnetic properties and solid state high-field EPR spectra of **2** over the range 50–420 GHz were investigated. The complex formation processes of L-Pro-FTSC with nickel(II) and zinc(II) have been studied in aqueous solution due to the excellent water solubility of the complexes via pH-potentiometry, UV−vis and ^{1}H NMR spectroscopy. The results of the antiproliferative activity *in vitro* showed that dimethylation improves the cytotoxicity and hR2 RNR inhibition. Therefore introduction of more lipophilic groups into thiosemicarbazone-proline backbone becomes an option for the synthesis of more efficient cytotoxic agents of this family of compounds.

Introduction

Thiosemicarbazones (TSCs) are known as versatile ligands for various metal ions.[1] Especially their first row transition metal coordination chemistry is well developed.[2] Specific feature of TSCs and their metal complexes is their broad spectrum of biological properties including antiviral, antibacterial, antimalarial, antifungal and anticancer activity.[3,4,5,6] α-*N*-heterocyclic TSCs (HCTs) are known for their anticancer activity since the 1950s when 2-formylpyridine thiosemicarbazone was discovered to possess *in vivo* antileukemic activity in a mice model.[7] The best studied HCT to date is 3-aminopyridine-2-carboxaldehyde thiosemicarbazone (3-AP), also referred to as Triapine, which has already been examined in several clinical phase I and II trials.[8,9,10] Triapine was found to be safe and effective against hematologic malignancies, e.g. leukemia.[11,12] A recent clinical phase II study including 37 patients with aggressive myeloproliferative neoplasms is of particular note since a response rate of 49% and complete remission in 24% of all patients has been documented.[13] However, other clinical phase II studies showed that Triapine is ineffective against a variety of solid tumors including pancreatic, adeno-, lung and renal carcinoma.[14,15,16,17] In the 1970s it was discovered that HCTs are inhibitors of the enzyme ribonucleotide reductase (RNR),[18,19] which catalyzes the rate determining step of DNA synthesis, namely the reduction of ribonucleotides to the corresponding 2'-deoxyribonucleotides.[20] Several mechanisms of RNR inhibition by thiosemicarbazones and especially Triapine have been proposed.[18,21] The until recently favored mechanistic scheme was that Triapine forms an iron(III) complex within the cell, which is reduced to Fe(II)-Triapine by intracellular reductants. Then the iron(II) complex reacts with oxygen, which leads to the formation of reactive oxygen species (ROS) able to quench the RNR's tyrosyl radical.[22,23,24] However, quite recently it was found that quenching of the tyrosyl radical is not oxygen dependent, suggesting that it might be reduced directly by the Fe(II)-Triapine complex without involvement of ROS.[25]

A second known target for HCTs is topoisomerase IIα (Topo IIα) an enzyme which controls the DNA topology during cell division by inducing temporary double strand breaks.[26,27,28,29] A series of Topo IIα inhibiting HCTs showed high affinity for the enzymes ATP binding pocket, thus acting as catalytic inhibitor of Topo IIα without the generation of DNA double strand breaks.[30] Although the structure–activity relationships (SARs) for HCTs Topo IIα inhibition are far from being completely understood, it was suggested that reaction with

copper(II) leading to square-planar complexes enhances the Topo IIα inhibition rate significantly.[31]

Nickel(II)-TSC complexes gained attention in the past few years. The reasons for this are the versatile coordination geometry preferences of this metal ion (square-planar, octahedral, tetrahedral), the formation of monomeric and dimeric complexes and its ability to mimic to some extent platinum(II), which is of great importance in chemotherapy.[32,33,34,35,36,37] The latter, however, is characterized by quite different ligand exchange rate constants.[38] Some salicylaldehyde TSC based nickel(II) complexes exhibited higher cytotoxicity than cisplatin (cis-diamminedichloridoplatinum(II), CDDP) in human cancer cell lines, while they were relatively nontoxic in normal kidney cells, demonstrating the potential of nickel(II)-TSC complexes for clinical development.[39] Zinc(II) shows low systemic cytotoxicity and forms easily TSC complexes. Moreover, the cytotoxicity of the zinc(II) complex is often enhanced compared to the free ligand.[40,41] A HCT based zinc(II) complex showed comparable cytotoxicity to 5-fluorouracil in human cancer cell lines[41] and a polyhydroxybenzaldehyde TSC based zinc(II) complex inhibited topoisomerase I.[42]

One of the great challenges in the design of new TSCs as possible anticancer compounds is to find the optimal balance between lipophilicity and water-solubility without losing efficacy. Increased bioactivity has been reported in the literature in many cases due to the higher lipophilicity of potential drugs.[Showell, G. A.; Mills, J. S. *Drug Discovery Today* **2003**, *8*, 551–556.; Akama, T.; Ishida, H.; Kimura, U.; Gomi, K.; Saito, H. *J. Med. Chem.* **1988**, *41*, 2056–2067.] However, high lipophilicity often leads to low aqueous solubility, which makes administration difficult and might limit the attainment of the proper concentration of the drug needed for the desired pharmacological response. In addition, low solubility precludes studies in aqueous solution, which are of utmost importance for investigations into the mode of action of these compounds. Low aqueous solubility of TSCs is a common feature, that explains the limited number of studies in aqueous solution reported so far.[43,44,45,46,47] From the other side aqueous solubility has influence on a compound's bioavailability through solubility-limited absorption, but is important for validation of *in vitro* antiproliferative activity assays.[48]

We reported recently on the first proline-TSC hybrids (L- and D-Pro-FTSC) and their copper(II) complexes.[49] These compounds are highly water-soluble. However, they exhibited

only moderate to low cytotoxicity (IC_{50} ≈ 100 μM in CH1 cell line for the copper(II) complexes, >300 μM for the free ligands), when compared with other HCTs that showed IC_{50} values in the nanomolar range.[50,51,52] This low cytotoxicity is presumably caused by the very low lipophilicity of these compounds, which may hinder cell membrane passage. Nevertheless, complex formation with copper(II) had a favorable effect on antiproliferative activity. We decided to extend our work and study the effect of other metal ions on cytotoxicity of L- and D-Pro-FTSC and that of dimethylation of terminal aminogroup in previously reported hybrids and their metal complexes. Dimethylation at terminal nitrogen of other HCTs was reported to increase the cytotoxicity.[53,54]

Herein we report on the synthesis of a new chiral ligand dm-L-Pro-FTSC or (*S*)-H_2L^2, along with two optically pure enantiomers L-Pro-FTSC and D-Pro-FTSC reported previously, and on six new nickel(II), copper(II) and zinc(II) complexes (**1–3** and **6–8**), in addition to two previously reported copper(II) complexes (**4** and **5**) (Chart 1).

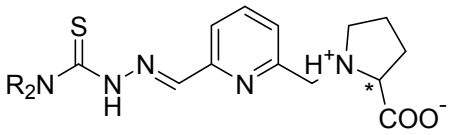

R = H, * = S, L-Pro-FTSC ((*S*)-$\mathbf{H_2L^1}$)
R = H, * = R, D-Pro-FTSC ((*R*)-$\mathbf{H_2L^1}$)
R = CH_3, * = S, dm-L-Pro-FTSC ((*S*)-$\mathbf{H_2L^2}$)

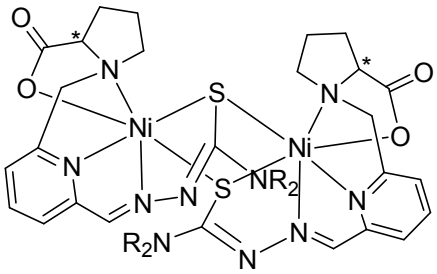

R = H, * = *S*, [Ni(L-Pro-FTSC-2H)]$_2$ (**1**)
R = H, * = *R*, [Ni(D-Pro-FTSC-2H)]$_2$) (**2**)
R = CH_3, * = *S*, [Ni(dm-L-Pro-FTSC-2H)]$_2$ (**3**)

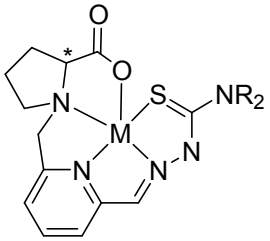

M = Cu, R = H, * = *S*, [Cu(L-Pro-FTSC-2H)] (**4**)
M = Cu, R = H, * = *R*, [Cu(D-Pro-FTSC-2H)] (**5**)
M = Cu, R = CH_3, * = *S*, [Cu(dm-L-Pro-FTSC-2H)] (**6**)
M = Zn, R = H, * = *S*, [Zn(L-Pro-FTSC-2H)] (**7**)
M = Zn, R = H, * = *R*, [Zn(D-Pro-FTSC-2H)] (**8**)

Chart 1. L- and D-Pro-FTSC and dm-L-Pro-FTSC and their metal complexes studied in this work. Underlined numbers indicate complexes investigated by X-ray diffraction. Co-crystallized solvent is not included in the formulas (see Experimental section).

The compounds were characterized by analytical and spectroscopic methods, magnetic susceptibility and EPR measurements (**1**) and X-ray diffraction (**1–3**, **6** and **7**). Solution equilibria of the nickel(II) and zinc(II) complexes formed with L-Pro-FTSC were studied in detail by the combination of various methods such as pH-potentiometry, UV−vis and ^{1}H NMR spectroscopy in order to determine the stoichiometry and the thermodynamic stability of complexes formed in aqueous solution. Complexation of these bivalent metal ions is compared to that of copper(II). Finally, the antiproliferative activity and hR2 RNR inhibiting activity of new compounds was assayed and discussed.

Experimental

Chemicals. 2,6-Dihydroxymethylpyridine and L-proline methylester hydrochloride were purchased from Alfa Aesar, while D-proline methylester hydrochloride from Acros Organics. Solvents were dried using standard procedures if needed.[55] 2-Hydroxymethyl-6-chloromethylpyridine and 6-chloromethylpyridine-2-carboxaldehyde were synthesized according to published procedures.[56] KOH and 4-(2-hydroxyethyl)-1-piperazineethanesulfonic acid (HEPES) were Sigma-Aldrich and HCl, KCl, $NiCl_2$ and $ZnCl_2$ were Reanal products. Nickel(II) and zinc(II) stock solutions were prepared by dissolving the appropriate amount of the metal chlorides in known amount of HCl and their concentrations were determined by complexometry via the EDTA complexes. Accurate strong acid content of the metal stock solutions were calculated on the basis of pH-potentiometric titrations.

Synthesis of ligands

D- and L-Pro-FTSC were synthesized as described elswhere.[49]

dm-L-Pro-FTSC·H_2O·0.2EtOH. (*S*)-1-[(6-Formylpyridin-2-yl)methyl]pyrrolidine-2-carboxylic acid (0.30 g, 1.28 mmol) and 4,4-dimethyl-3-thiosemicarbazide (0.15 g, 1.28 mmol) were dissolved in dry ethanol (6 mL) and the reaction mixture was stirred at room temperature for 24 h. The white precipitate formed was filtered off under inert atmosphere, washed with dry ethanol and dried in vacuo. Yield: 0.17 g, 39%. Anal. Calcd for $C_{15}H_{21}N_5O_2S·H_2O·0.2C_2H_5OH$ (M = 362.65 g/mol): C, 51.00; H, 6.73; N, 19.31; S, 8.84. Found: C, 50.84; H, 6.56; N, 19.01; S, 8.68. *E-isomer*: ^{1}H NMR (500 MHz, DMSO-d_6) δ 11.20 (s, 1H, H^2), 8.21 (s, 1H, H^{13}), 7.88 – 7.77 (m, 2H, H^5, H^6), 7.45 (d, J = 7.0 Hz, 1H, H^4), 4.16 (d, J = 14.2 Hz, 1H, H^7), 3.90 (d, J = 14.2 Hz, 1H, H^7), 3.49 (dd, J = 8.9, 5.3 Hz, 1H, H^8), 3.13 – 3.06 (m, 1H, H^{11}), 2.66 – 2.58 (m, 1H, H^{11}), 2.19 – 2.05 (m, 1H, H^9), 1.96 – 1.67 (m, 3H, H^9, H^{11}). ^{13}C NMR (126 MHz, DMSO-d_6) δ 181.06 (Cq, C^{14}), 173.76 (Cq, C^{12}), 157.59 (Cq, C^3), 153.46 (Cq, C^1), 144.17 (CH, C^{13}), 137.81 (CH, C^5), 123.55 (CH, C^4), 118.64 (CH, C^6), 66.23 (CH, C^8), 59.13 (CH_2, C^7), 53.54 (CH_2, C^{11}), 42.76 ($2CH_3$, C^{15}, C^{16}), 29.28 (CH_2, C^9), 23.71,(CH_2, C^{10}). *Z-isomer*: ^{1}H NMR (500 MHz, DMSO-d_6) δ 14.75 (s, 1H, H^2), 8.05 (t, J = 7.8 Hz, 1H, H^5), 7.62 (m, 2H, H^4, H^6), 7.58 (s, 1H, H^{13}), 4.10 (d, J = 14.1 Hz, 1H, H^7), 3.79 (d, J = 14.0 Hz, 1H, H^7), 3.51 – 3.42 (m, 1H, H^8), 2.96 – 2.90 (m, 1H, H^{11}), 2.56 – 2.43 (m, 1H, H^{11}, overlapped with residual DMSO signal), 2.19 – 2.05 (m, 1H, H^9),

1.96 – 1.67 (m, 3H, H^9, H^{10}). ^{13}C NMR (126 MHz, DMSO-d_6) δ 180.61 (Cq, C^{14}), 174.92 (Cq, C^{12}), 158.33 (Cp, C_3), 151.60 (Cq, C^1), 139.26 (CH, C^5), 136.65, (CH, C^{13}), 124.96 (CH, C^6), 124.03 (CH, C^4), 65.29 (CH, C^8), 59.41 (CH_2, C^7), 53.32 (CH_2, C^{11}), 40.61 ($2CH_3$, C^{15}, C^{16}, overlapped with residual DMSO signal), 29.33 (CH_2, C^9), 23.43 (CH_2, C^{10}). For atom numbering and structures of *E* and *Z* isomers see Figure S2. Solubility in water: ≥ 413 mg/mL. ESI-MS (methanol), positive: *m*/*z* 336 ($[M + H]^+$). IR (ATR, selected bands, ν_{max}): 3156, 2963, 1643, 1579, 1547, 1517, 1445, 1346, 1266, 1080, 831, 683, 592 cm^{-1}.

Synthesis of metal complexes

[Ni(L-Pro-FTSC−2H)]$_2$·2H$_2$O·MeOH (**1**·2H_2O·MeOH). To a solution of L-Pro-FTSC (0.10 g, 0.33 mmol) in water (15 mL) was added a solution of nickel(II) acetate tetrahydrate (0.16 g, 0.66 mmol) in water (5 mL). The mixture was heated at 70 °C for 1 h and then stirred at room temperature overnight. The resulted brown solution of the raw product in water was subjected to preparative HPLC (MeOH/H_2O). Slow diffusion of diethyl ether into a methanolic solution of the purified product gave brown crystals which were filtered off, washed with a diethyl ether/methanol 5 : 1 mixture and dried in vacuo. Yield: 0.07 g, 54%. Anal. Calcd for $C_{26}H_{30}Ni_2N_{10}O_4S_2·2H_2O·CH_3OH$ (*M* = 796.17 g/mol): C, 40.73; H, 4.81; N, 17.59; S, 8.05. Found: C, 40.49; H, 4.51; N, 17.35; S, 7.77. Solubility in water: ≥ 10.3 mg/mL. ESI-MS (methanol), positive: *m*/*z* 364 ($[½M + H]^+$), 386 ($[½M + Na)]^+$). IR (ATR, selected bands, ν_{max}): 3294, 1588, 1459, 1162, 785, 668, 605 cm^{-1}.

[Ni(D-Pro-FTSC−2H)]$_2$·3.7H$_2$O·MeOH (**2**·3.7H_2O·MeOH). To a solution of D-Pro-FTSC (0.17 g, 0.55 mmol) in water (30 mL) was added a solution of nickel(II) acetate tetrahydrate (0.28 g, 1.11 mmol) in water (10 mL). The mixture was heated at 70 °C for 1 h and then stirred at room temperature overnight. The resulted brown solution of the raw product in water was subjected to preparative HPLC (MeOH/H_2O). Slow diffusion of diethyl ether into a methanolic solution of the purified product gave brown crystals which were filtered off, washed with a diethyl ether/methanol 5 : 1 mixture and dried in vacuo. Yield: 0.13 g, 65%. Anal. Calcd for $C_{26}H_{30}Ni_2N_{10}O_4S_2·3.7H_2O·CH_3OH$ (*M* = 826.78 g/mol): C, 39.22; H, 5.04; N, 16.94; S, 7.75. Found: C, 39.00; H, 4.65; N, 17.08; S, 7.37. Solubility in water: ≥ 10.3 mg/mL. ESI-MS (methanol), positive: *m*/*z* 364 ($[½M + H]^+$), 386 ($[½M + Na)]^+$). IR (ATR, selected bands, ν_{max}): 3294, 1588, 1459, 1162, 785, 668, 605 cm^{-1}.

[Ni(dm-L-Pro-FTSC–2H)]$_2$·0.2H$_2$O·3.6MeOH (**3**·0.2H_2O·3.6MeOH). (*S*)-1-[(6-Formyl-pyridin-2-yl)methyl]pyrrolidine-2-carboxylic acid (0.19 g, 0.81 mmol), 4,4-dimethyl-3-thiosemicarbazide (0.10 g, 0.81 mmol) and nickel(II) acetate tetrahydrate (0.21 g, 0.86 mmol) were dissolved in dry ethanol (12 mL) in a 25 mL Schlenk tube. The mixture was stirred at 70 °C overnight. The next day a grey precipitate of [Ni(4,4-dimethyl-3-thiosemicarbazide)$_2$] was filtered off. The filtrate was subjected to preparative HPLC (MeOH/H_2O). Slow diffusion of diethyl ether into a methanolic solution of the purified product gave dark brown crystals which were filtered off, washed with a diethyl ether/methanol 5 : 1 mixture and dried in vacuo. Yield: 0.09 g, 27%. Anal. Calcd for $C_{30}H_{38}Ni_2N_{10}O_4S_2$·0.2$H_2O$·3.6$CH_3OH$ (*M* = 903.16 g/mol): C, 44.69; H, 5.89; N, 15.51; S, 7.10. Found: C, 44, 35; H, 5.65; N, 15.85; S, 6.79. Solubility in water: ≥ 15.3 mg/mL. ESI-MS (methanol), positive: *m*/*z* 392 ([½M + H]$^+$). IR (ATR, selected bands, ν_{max}): 3384, 2922, 1593, 1507, 1362, 1253, 1129, 909, 805, 677 cm^{-1}.

Complexes **[Cu(L-Pro-FTSC–2H)]** (**4**) and **[Cu(D-Pro-FTSC–2H)]** (**5**) were prepared by following a recently published protocol.[49]

[Cu(dm-L-Pro-FTSC–2H)]·H$_2$O·0.2MeOH (**6**·H_2O·0.2MeOH). (*S*)-1-[(6-Formylpyridin-2-yl)methyl]pyrrolidine-2-carboxylic acid (0.30 g, 1.28 mmol), 4,4-dimethyl-3-thiosemicarbazide (0.15 g, 1.28 mmol) and copper(II) acetate monohydrate (0.27 g, 1.36 mmol) were dissolved in dry ethanol (10 mL) in a 50 mL Schlenk tube. The mixture was stirred at 70 °C overnight. The resulted green solution of the raw product in water was subjected to preparative HPLC (MeOH/H_2O). Slow diffusion of diethyl ether into a methanolic solution of the purified product gave green crystals which were filtered off, washed with a diethyl ether/methanol 5 : 1 mixture and dried in vacuo. Yield: 0.19 g, 38%. Anal. Calcd for $C_{15}H_{19}CuN_5O_2S$·H_2O·0.2CH_3OH (*M* = 421.38 g/mol): C, 43.32; H, 5.21; N, 16.62; S, 7.60. Found: C, 43.46; H, 5.00; N, 16.46; S, 7.54. Solubility in water: ≥ 8.5 mg/mL. ESI-MS (methanol), positive: *m*/*z* 795 ([2M + H]$^+$), 817 ([2M+Na)]$^+$). IR (ATR, selected bands, ν_{max}): 3542, 3152, 2923, 1596, 1503, 1361, 1247, 1131, 910, 792, 625 cm^{-1}.

[Zn(L-Pro-FTSC–2H)]·1.9H$_2$O (**7**·1.9H_2O). To a solution of L-Pro-FTSC (0.12 g, 0.39 mmol) in water (15 mL) was added a solution of zinc(II) acetate dihydrate (0.17 g, 0.78 mmol) in water (5 mL). The mixture was heated at 70 °C for 1 h. After cooling down the solution was concentrated under reduced pressure to about 5 mL and allowed to stand at 4 °C overnight. Yellow, needle-like crystals were filtered off, washed with cold water and dried in

vacuo. Yield: 0.13 g, 65%. Anal. Calcd for $C_{13}H_{15}N_5O_2SZn \cdot 1.9H_2O$ (M = 404.98 g/mol): C, 38.56; H, 4.68; N, 17.29; S, 7.92%. Found: C, 38.75; H, 4.29; N, 16.98; S, 8.04%. ^{1}H NMR (500 MHz, DMSO-d_6) δ 8.22 (s, 1H, H^{12}), 8.08 (t, J = 7.7 Hz, 1H, H^4), 7.62 (d, J = 7.5 Hz, 1H, H^5), 7.57 (s, 2H, $H^{3'}$), 7.42 (d, J = 7.6 Hz, 1H, H^3), 4.34 (d, J = 16.8 Hz, 1H, H^6), 4.08 (d, J = 16.9 Hz, 1H, H^6), 3.50 (m, 1H, H^{10}), 3.25 – 3.12 (m, 1H, H^7), 2.99 – 2.86 (m, 1H, H^{10}), 2.32 (m, 1H, H^8), 1.95 (m, 1H, H^9), 1.79 (m, 2H, H^8, H^9) ppm. ^{13}C NMR (125 MHz, DMSO-d_6) δ 183.96 (Cq, C^{13}), 177.11 (Cq, C^{11}), 156.16 (Cq, C^1), 149.78 (Cq, C^2), 143.04 (CH, C^4), 135.15 (CH, C^{12}), 123.05 (CH, C^3), 123.01 (CH, C^5), 72.48 (CH, C^7), 60.82 (CH_2, C^6), 58.57 (CH_2, C^{10}), 31.38 (CH_2, C^8), 24.98 (CH_2, C^9) ppm. Solubility in water: ≥ 1.4 mg/mL. ESI-MS (methanol), positive: m/z 370 ($[M + H]^+$), 392 ($[M + Na)]^+$). IR (ATR, selected bands, ν_{max}): 3287, 1596, 1454, 1155, 1076, 1009, 904, 781, 656, 605 cm^{-1}.

[Zn(D-Pro-FTSC−2H)]·2.6H$_2$O (**8**·2.6H$_2$O). To a solution of D-Pro-FTSC (0.15 g, 0.49 mmol) in water (20 mL) was added a solution of zinc(II) acetate dihydrate (0.22 g, 0.98 mmol) in water (5 mL). The mixture was heated at 70 °C for 1 h. After cooling down the solution was concentrated under reduced pressure to about 5 mL and allowed to stand at 4 °C overnight. Yellow, needle-like crystals were filtered off, washed with cold water and dried in vacuo. Yield: 0.06 g, 33%. Anal. Calcd for $C_{13}H_{15}N_5O_2SZn \cdot 2.6H_2O$ (M = 417.59 g/mol): C, 37.39; H, 4.88; N, 16.77; S, 7.68. Found: C, 37.64; H, 4.87; N, 16.41; S, 7.30. ^{1}H NMR (500 MHz, DMSO-d_6) δ 8.22 (s, 1H, H^{12}), 8.08 (t, J = 7.7 Hz, 1H, H^4), 7.62 (d, J = 7.5 Hz, 1H, H^5), 7.57 (s, 2H, $H^{3'}$), 7.42 (d, J = 7.6 Hz, 1H, H^3), 4.34 (d, J = 16.8 Hz, 1H, H^6), 4.08 (d, J = 16.9 Hz, 1H, H^6), 3.50 (m, 1H, H^{10}), 3.25 – 3.12 (m, 1H, H^7), 2.99 – 2.86 (m, 1H, H^{10}), 2.32 (m, 1H, H^8), 1.95 (m, 1H, H^9), 1.79 (m, 2H, H^8, H^9) ppm. ^{13}C NMR (125 MHz, DMSO-d_6) δ 183.96 (Cq, C^{13}), 177.11 (Cq, C^{11}), 156.16 (Cq, C^1), 149.78 (Cq, C^2), 143.04 (CH, C^4), 135.15 (CH, C^{12}), 123.05 (CH, C^3), 123.01 (CH, C^5), 72.48 (CH, C^7), 60.82 (CH_2, C^6), 58.57 (CH_2, C^{10}), 31.38 (CH_2, C^8), 24.98 (CH_2, C^9) ppm. Solubility in water: ≥ 1.4 mg/mL. ESI-MS (methanol), positive: m/z 370 ($[M + H]^+$), 392 ($[M + Na)]^+$). IR (ATR, selected bands, ν_{max}): 3287, 1596, 1454, 1155, 1076, 1009, 904, 781, 656, 605 cm^{-1}.

pH-potentiometric measurements. The exact concentration of the stock solutions of the L-Pro-FTSC was determined from pH-potentiometric titrations by using the computer program HYPERQUAD.[57] The pH-metric measurements for the determination of the proton dissociation constants of the L-Pro-FTSC and the overall stability constants of the metal complexes were carried out at 298.0 ± 0.1 K in water and at an ionic strength of 0.10 M KCl to keep the

activity coefficients constant. The titrations were performed with carbonate-free KOH solution of known concentration (0.10 M). The concentrations of the base and the HCl were determined by pH-potentiometric titrations. An Orion 710A pH-meter equipped with a Metrohm combined electrode (type 6.0234.100) and a Metrohm 665 Dosimat burette were used for the titrations. The electrode system was calibrated to the pH = $-\log[H^+]$ scale according to the method suggested by Irving *et al*.[58] The average water ionization constant, pK_w, is 13.76 ± 0.01, which corresponds well to the literature data.[59] The reproducibility of the titration points included in the calculations was within 0.005 pH. The pH-metric titrations were performed in the pH range 2.0 − 11.5. The initial volume of the samples was 5.0 mL. The ligand concentration was 2 mM and metal ion-to-ligand ratios of 1:1 − 1:4 were used. The accepted fitting of the titration curves was always less than 0.01 mL. Samples were deoxygenated by bubbling purified argon through them for approximately 10 min prior to the measurements. Argon was also passed over the solutions during the titrations.

The protonation constants of the L-Pro-FTSC were determined with the computer program HYPERQUAD.[57] PSEQUAD[60] was utilized to establish the stoichiometry of the complexes and to calculate the stability constants ($\log\beta(M_pL_qH_r)$). $\beta(M_pL_qH_r)$ is defined for the general equilibrium $pM + qL + rH \rightleftharpoons M_pL_qH_r$ as $\beta(M_pL_qH_r) = [M_pL_qH_r]/[M]^p[L]^q[H]^r$, where M denotes the metal ion and L the completely deprotonated ligand. In all calculations exclusively titration data were used from experiments in which no precipitate was visible in the reaction mixture.

UV–vis spectrophotometric, CD and ^{1}H NMR measurements. A Hewlett Packard 8452A diode array spectrophotometer was used to record the UV–vis spectra in the 200 to 800 nm window. The path length was 0.5 or 1.0 cm. The spectrophotometric titrations were performed on samples of the L-Pro-FTSC alone or with nickel(II) ions; the concentration of the ligand was ~100 μM and the metal-to-ligand ratios were 1:1 and 1:2 over the pH range between 2 and 11.5 at an ionic strength of 0.10 M (KCl) in water at 298.0 ± 0.1 K. Measurements for the nickel(II) − L-Pro-FTSC systems at metal-to-ligand ratio 1:1 were also carried out at various concentrations (1 μM – 0.8 mM) and at pH 7.4 (20 mM HEPES buffer).

One dimensional ^{1}H and ^{13}C NMR and two dimensional ^{1}H-^{1}H COSY, ^{1}H-^{1}H TOCSY, ^{1}H-^{1}H TOCSY, ^{1}H-^{1}H ROESY or ^{1}H-^{1}H NOESY, ^{1}H-^{13}C HSQC and ^{1}H-^{13}C HMBC NMR spectra

were recorded on two Bruker Avance III instruments. DMSO-d_6 or $CDCl_3$ were used as solvent. ^1H or ^{13}C chemical shifts were measured relatively to the residual solvent peaks. The pH-dependent ^1H NMR studies were carried out on a Bruker Ultrashield 500 Plus instrument. 4,4-Dimethyl-4-silapentane-1-sulfonic acid was used as an internal NMR standard and WATERGATE method was used to suppress the solvent resonance. L-Pro-FTSC was dissolved in a 10% (v/v) D_2O/H_2O mixture in a concentration of 1 mM, the zinc(II)-to-ligand ratios were 1:1 and 1:2 and the nickel(II)-to-ligand ratio was 1:1 at 298 K. PSEQUAD[60] was used to calculate the pK value of the complex $[ZnLH]^+$. ^1H NMR spectra were recorded for the zinc(II) − L-Pro-FTSC (1:1) system at 1 mM concentration in the presence of 630 μM HSA at pH 7.40 (20 mM HEPES buffer, 0.1 M KCl) or in MEM at 298 K after 24 h incubation.

CD spectra for the nickel(II) and zinc(II) complexes of L-Pro-FTSC and D-Pro-FTSC were recorded on a Jasco J-815 spectrometer in the wavelength interval from 230 to 600 nm. Samples contained 0.500 mM nickel(II) or 0.025 mM zinc(II) complex at pH 7.4 (20 mM HEPES buffer, 0.1 M KCl) using optical cells of 0.2 or 0.5 cm path lengths, respectively. CD data are given as the differences in molar absorptivities between left and right circularly polarized light, based on the concentration of the ligand ($\Delta\varepsilon = \Delta A / l / c_{\text{ligand or complex}}$).

Determination of the distribution coefficient (*D*). $D_{7.4}$ values of the zinc(II) and nickel(II) complexes of L- and D-Pro-FTSC, as well as of dm-L-Pro-FTSC (**3**, **6–8**) were determined by the traditional shake-flask method in *n*-octanol/buffered aqueous solution at pH 7.4 (20 mM HEPES buffer) at 298.0 ± 0.2 K as described previously,[49] and compared to those of metal-free hybrids. Two parallel experiments were performed for each sample. The complexes were dissolved in 0.1 mM in the *n*-octanol pre-saturated aqueous solution of the buffer at constant ionic strength (0.10 M KCl). The aqueous solutions and *n*-octanol with 1:1 phase ratio were gently mixed with 360° vertical rotation for 3 h to avoid the emulsion formation, and the mixtures were centrifuged at 5000 rpm for 3 min by a temperature controlled centrifuge (Sanyo) at 298 K. After separation UV−vis spectra of the complexes in the aqueous phase were compared to those of the original aqueous solutions. $D_{7.4}$ values of the metal complexes were calculated as the mean of [Absorbance (original solution) / Absorbance (aqueous phase after separation) – 1] obtained at the λ_{max} values (360 nm for the zinc(II), 375 or 380 nm for the nickel(II) and 396 nm for the copper(II) complexes). When no measurable amount of the

complexes was found in the *n*-octanol phase, $D_{7.4}$ values for those compounds were merely estimated.

Crystallographic Structure Determination. X-ray diffraction measurements were performed on Bruker X8 APEXII CCD and Bruker D8 VENTURE diffractometers. Single crystals were positioned at 40, 35, 100, 35 and 40 mm from the detector, and 561, 772, 2147, 2797 and 815 frames were measured, each for 100, 4, 24, 4 and 30 s over 1, 0.4, 0.4, 0.4 and 1° scan width for **1**·3.25CH_3OH, **2**·4CH_3OH, **3**·2.88CH_3OH, **6**·H_2O and **7**·CH_3OH, correspondingly. The data were processed using SAINT software.[61] Crystal data, data collection parameters, and structure refinement details are given in Table 1. The structures were solved by direct methods and refined by full-matrix least-squares techniques. Non-H atoms were refined with anisotropic displacement parameters. H atoms were inserted in calculated positions and refined with a riding model. Co-crystallized methanol in **3**·2.88CH_3OH was found in part disordered. The disorder was solved by using SADI instructions implemented in SHELXL-97, while the atoms involved were refined with isotropic displacement parameters and the positions of H atoms were not calculated. One methanol molecule from two crystallographically independent in the structure of **7**·CH_3OH was found disordered over two positions with s.o.f. 0.6 : 0.4. The following computer programs were used: structure solution, *SHELXS-97* and refinement, *SHELXL-97*;[62] molecular diagrams, *ORTEP*.[63]

Table 1. Crystal data and details of data collection for **1**·3.25CH_3OH, **2**·4CH_3OH, **3**·2.88CH_3OH, **6**·H_2O and **7**·CH_3OH.

	1·3.25CH_3OH	**2**·4CH_3OH	**3**·2.88CH_3OH	**6**·H_2O	**7**·CH_3OH
empirical formula	$C_{29.25}H_{43.5}N_{10}Ni_2O_{7.75}S_2$	$C_{30}H_{46}N_{10}Ni_2O_8S_2$	$C_{32.88}H_{49.5}N_{10}Ni_2O_{6.88}S_2$	$C_{15}H_{21}CuN_5O_3S$	$C_{14}H_{19}N_5O_3SZn$
Fw	840.78	856.31	677.09	414.97	725.05
space group	$P2_12_12_1$	$P2_12_12_1$	$P2_12_12_1$	$P2_12_12_1$	$P2_1$
A [Å]	13.1049(7)	13.2489(4)	11.7885(13)	6.6987(7)	8.2454(4)
B [Å]	15.1240(13)	15.2821(5)	11.8487(13)	13.3713(18)	11.8012(6)
C [Å]	18.0808(16)	17.9458(7)	55.473(6)	18.755(2)	16.8293(7)
α [°]					
β [°]					93.338(3)
γ [°]					
V [Å^3]	3583.6(5)	3633.5(2)	7748.4(15)	1679.9(4)	1634.81(13)
Z	4	4	8	4	4
λ [Å]	0.71073	0.71073	0.71073	0.71073	0.71073
ρ_{calcd} [g cm^{-3}]	1.558	1.565	1.502	1.641	1.636
crystal size, mm	0.10 × 0.02 × 0.01	0.22 × 0.18 × 0.11	0.37 × 0.28 × 0.05	0.46 × 0.25 × 0.23	0.07 × 0.07 × 0.04
T [K]	120(2)	100(2)	100(2)	100(2)	120(2)
μ [mm^{-1}]	1.230	1.215	1.139	1.451	1.654
R_1[a]	0.0603	0.0316	0.0405	0.0189	0.0408
wR_2[b]	0.1373	0.0661	0.1081	0.0522	0.0647
GOF[c]	1.010	1.034	1.092	1.010	1.019
Flack parameter	–0.04(2)	0.001(7)	0.03(1)	–0.009(6)	0.008(9)

[a] $R_1 = \Sigma||F_o| - |F_c||/\Sigma|F_o|$. [b] $wR_2 = \{\Sigma[w(F_o^2 - F_c^2)^2]/\Sigma[w(F_o^2)^2]\}^{1/2}$. [c] GOF = $\{\Sigma[w(F_o^2 - F_c^2)^2]/(n - p)\}^{1/2}$, where n is the number of reflections and p is the total number of parameters refined.

Magnetic Measurements and EPR Spectroscopy. Magnetic susceptibility data (2–300 K) were collected on powdered samples using a SQUID magnetometer (Quantum Design MPMS-XL) at 0.1 T. The temperature dependence of the magnetic susceptibility for dinuclear nickel(II) cluster **1** was analyzed according to the Hamiltonian (eq 1),[64]

$$\hat{\boldsymbol{H}} = -2J\,\hat{\boldsymbol{S}}_1\cdot\hat{\boldsymbol{S}}_2 + \mu_B\boldsymbol{B}\,\{\boldsymbol{g}_1\}\,\hat{\boldsymbol{S}}_1 + \hat{\boldsymbol{S}}_1\,\{\boldsymbol{D}_1\}\,\hat{\boldsymbol{S}}_1 + \mu_B\boldsymbol{B}\,\{\boldsymbol{g}_2\}\,\hat{\boldsymbol{S}}_2 + \hat{\boldsymbol{S}}_2\,\{\boldsymbol{D}_2\}\,\hat{\boldsymbol{S}}_2 + \hat{\boldsymbol{S}}_1\,\{\boldsymbol{D}_{12}\}\,\hat{\boldsymbol{S}}_2 \quad (1),$$

in which $\{\boldsymbol{g}_1\}$ *and* $\{\boldsymbol{g}_2\}$ represent the local *g* matrices, $\{\boldsymbol{D}_1\}$ *and* $\{\boldsymbol{D}_2\}$ are the local single-ion zfs tensors and the $\{\boldsymbol{D}_{12}\}$ term contains the magnetic dipolar interactions along with the anisotropic exchange interactions between the metal ions. The more commonly used zfs parameters *D* and *E* are related to the tensor components by eq 2:

$$D = (2D_{zz} - D_{xx} - D_{yy}) / 2, \qquad E = (D_{xx} - D_{yy}) / 2 \qquad (2)$$

These formulas are valid for each of the $\{D\}$ quantities in eq 1.

To obtain a manageable model it was assumed that the two Ni ions are equivalent, which is not strictly correct. Different orientation of the $\{\boldsymbol{D}_1\}$ and $\{\boldsymbol{D}_2\}$ tensors was taken into account, as the *Z* axes of the two D tensors are tilted by 26 deg from each other according to the DFT calculations (see the DFT section below), but the corresponding components of $\{\boldsymbol{D}_1\}$ and $\{\boldsymbol{D}_2\}$ were assumed equal. These {D} tensor components were not fitted but were calculated from the *D* and *E* values in the $S = 2$ state found from EPR (below). The spin Hamiltonian matrix was diagonalised to find the energy levels and the magnetic susceptibility per mole of dimer was calculated from eq 3:

$$\chi_d = -\frac{N}{B}\frac{\sum_i \frac{\partial E_i}{\partial B}\exp(-E_i/kT)}{\sum_i \exp(-E_i/kT)} \qquad (3)$$

The derivatives $\delta E_i/\delta B$ were evaluated numerically by calculating the energy levels slightly below and slightly above (±5 Gauss) the operational magnetic field of a SQUID magnetometer (1000 G in our case).

The terms $\{D_1\}$ and $\{D_2\}$ represents the usual Zero-Field Splitting (ZFS) of the $^3A_2$ ground state of Ni(II).[65]

This and similar models have been widely used to characterize magnetic interaction in different dinuclear nickel(II) complexes.[65,66,67] We also allowed an interdimer exchange term (zJ') in the molecular field approximation[68] according to the eq. 4:

$$\chi' = \frac{\chi}{1 - \left({2zJ'}/{Ng^2\mu_B^2} \right)\chi} \qquad (4)$$

The X-band (9.5 GHz) EPR spectra were recorded at 20 K on a Bruker Elexsys-II EPR spectrometer with an Oxford Instruments ESR900 helium cryostat under the following conditions: microwave power 3.2 mW, modulation amplitude 5 G, modulation frequency 100 kHz, conversion time 29.3 ms. The concentration of the tyrosyl radical was determined by double integration of EPR spectra recorded at nonsaturating microwave power levels, and compared with the copper standard (1 mM $CuSO_4$ in 10 mM EDTA). The calculated radical concentration was normalized and expressed in percent of the control sample. High-field, high-frequency EPR spectra at temperatures ranging from ca. 3 to 10 K were recorded on a home-built spectrometer at the EMR facility of the NHMFL.[69] The instrument is a transmission-type device in which microwaves are propagated in cylindrical lightpipes. The microwaves were generated by a phase-locked Virginia Diodes source generating frequency of 13 ± 1 GHz which was multiplied by a cascade of frequency doublers and/or triplers. A superconducting magnet (Oxford Instruments) capable of reaching a field of 17 T was employed.

We simulated EPR spectra of **1** using the "giant spin" approach, in which the spectra of the coupled states (S = 1 and S = 2) were analyzed separately in terms of the coupled-spin Hamiltonian (eq 5):

$$\hat{\boldsymbol{H}}_{\boldsymbol{S}} = \mu_B \boldsymbol{B} \cdot \{\boldsymbol{g}_S\} \cdot \hat{\boldsymbol{S}} + D[\hat{\boldsymbol{S}}_z^{\,2} - S(S+1)/3] + E(\hat{\boldsymbol{S}}_x^{\,2} - \hat{\boldsymbol{S}}_y^{\,2}) \qquad (5),$$

in which each of the spin states has its own zero-field splitting parameters D, E and g matrices which can be related to the single-ion parameters[64,70] corresponding to the spin Hamiltonian (1).

Cell lines and culture conditions. Human cervical carcinoma (HeLa), human melanoma (FemX), human alveolar basal adenocarcinoma (A549), human breast cancer (MDA-MB-453) cell lines and normal human fetal lung fibroblast cell line (MRC-5) were maintained as monolayer culture in the Roswell Park Memorial Institute (RPMI) 1640 nutrient medium (Sigma Chemicals Co, USA). RPMI 1640 nutrient medium was prepared in sterile deionized water, supplemented with penicillin (192 U/mL), streptomycin (200 mg/mL), 4-(2-hydroxyethyl) piperazine-1-ethanesulfonic acid (HEPES) (25 mM), L-glutamine (3 mM) and 10% of heat-inactivated foetal calf serum (FCS) (pH 7.2). The cells were grown at 37 ºC in 5% CO_2 in a humidified air atmosphere.

MTT assay. Antiproliferative activity of the investigated compounds was determined using 3-(4,5-dymethylthiazol-yl)-2,5-diphenyltetrazolium bromide (MTT, Sigma-Aldrich) assay.[71] Cells were seeded into 96-well cell culture plates (Thermo Scientific Nunc™), at a cell density of 3000 c/w (HeLa), 6000 c/w (A549), 4000 c/w (MDA-MD-453), 5000 c/w (FemX, MRC-5) in 100 μl of culture medium. After 24 h of growth, cells were exposed to the serial dilutions of the tested complexes. The investigated compounds were dissolved in DMSO at a concentration of 30 mM as stock solution, and prior the use diluted with nutrient medium to the desired final concentrations (in range from 18.75 up to 300 μM). Each concentration was tested in triplicates. Serial dilutions were made in culture medium so that the final concentration of DMSO per well was less than 1% (v/v) in all experiments. After incubation periods of 48 h, 20 μL of MTT solution (5 mg/mL in phosphate buffer solution, pH 7.2) were added to each well. Samples were incubated for 4 h at 310 K, with 5% CO_2 in a humidified atmosphere. Formazan crystals were

dissolved in 100 μL of 10% sodium dodecyl sulfate (SDS). Absorbances were recorded after 24 h, on an enzyme-linked immunosorbent assay (ELISA) reader (ThermoLabsystems Multiskan EX 200–240 V), at the wavelength of 570 nm. IC_{50} values (μM), were determined from the cell survival diagrams. The percentages of surviving cells relative to untreated controls were determined. The IC_{50} value, defined as the concentration of the compound causing 50% cell growth inhibition, was estimated from the dose-response curves.

Ribonucleotiode reductase inhibition

Sample preparation for EPR measurements. The tyrosyl radical reduction kinetics in human R2 RNR protein (hR2) by L-Pro-FTSC and dm-L-Pro-FTSC, as well as complexes **4**, **6**, and **7**, was monitored by EPR spectroscopy. Purified recombinant hR2 was obtained from the Department of Medical Biochemistry and Biophysics, Karolinska Institute, Sweden. The iron-reconstituted R2 protein contained 2 iron ions and 0.38 tyrosyl radicals per polypeptide. Samples containing 20 μM hR2 in Tris buffer, pH 7.60 / 100 mM KCl / 5% glycerol, 20 μM compound (1% (w/w) DMSO/H_2O), and 2 mM dithiothreitol (DTT) (only for experiments done in the presence of the reductant) were incubated at room temperature for designated times and quickly frozen in cold isopentane. The same sample was used for repeated incubations and was refrozen before each EPR measurement. The intrinsic decay of the tyrosyl radical, obtained from the control sample containing 20 μM hR2 in Tris buffer, pH 7.60 / 100 mM KCl / 5% glycerol, was subtracted at each time point.

Results and Discussion

Synthesis and Characterization of dm-L-Pro-FTSC. dm-L-Pro-FTSC was synthesized in six steps as shown in Scheme S1. The first five steps to the key-aldehyde **F** were described in detail previously.[49] Aldehyde **F** was then condensed in a Schiff-base reaction with 4,4-dimethyl-3-thiosemicarbazide in dry ethanol at room temperature. One dimensional ^1H and ^{13}C NMR and two dimensional ^1H-^1H COSY, ^1H-^1H TOCSY, ^1H-^1H NOESY, ^1H-^{13}C HSQC and ^1H-^{13}C HMBC NMR spectra were in agreement with the expected structure, enabling the assignment of

all ^{1}H and ^{13}C resonances (for atom numbering see Scheme S2 in the Supporting Information). dm-L-Pro-FTSC exists as a mixture of *E* and *Z* isomers in DMSO with a *E* : *Z* ratio of 1 : 0.39. The proton at the hydrazinic nitrogen N^2, in the *Z* configuration is involved in a hydrogen bond to the pyridine nitrogen leading to a strong downfield shift of its resonance signal from 11.20 to 14.75 ppm. The solvent dependent formation of *E* and *Z* isomers is well documented in the literature and our data is in good agreement with that reported for other α-pyridyl-TSCs.[72] The purity of the compound was further confirmed by elemental analysis. The ESI mass spectra recorded in a positive ion mode showed a strong peak at *m*/*z* 336 due to the $[M + H]^+$ ion.

Synthesis and Characterization of the Metal(II) Complexes. The zinc(II) and nickel(II) complexes of D- and L-Pro-FTSC were prepared similarly to the previously reported copper(II) complexes, by reaction of the metal(II) acetate hydrates with the ligand in aqueous solution. The nickel(II) and copper(II) complexes of dm-L-Pro-FTSC were prepared *in situ* by reaction of the aldehyde **F** with 4,4-dimethyl-3-thiosemicarbazide in the presence of the corresponding metal(II) acetate in dry ethanol. The structure of all metal(II) complexes (except [Zn(D-Pro-FTSC–2H)]) in the solid state was confirmed by single crystal X-ray diffraction. ESI-MS spectra of **1** and **2** recorded in a positive ion mode showed peaks at *m*/*z* 364 and 386 attributed to $[Ni(L\text{-Pro-FTSC}–2H) + H]^+$ or $[Ni(D\text{-Pro-FTSC}–2H) + H]^+$ and to $[Ni(L\text{-Pro-FTSC}–2H) + Na]^+$ or $[Ni(D\text{-Pro-FTSC}–2H) + Na]^+$, respectively, while that of **3** at *m*/*z* 392 due to $[Ni(dm\text{-L-Pro-FTSC}–2H) + H]^+$. Strong signals at *m*/*z* 795 and 817 in the mass spectrum of **6** were assigned to $[\{Cu(dm\text{-L-Pro-FTSC}–2H)\}_2 + H]^+$ and $[\{Cu(dm\text{-L-Pro-FTSC}–2H)\}_2 + Na]^+$, respectively, while those at *m*/*z* 370 and 392 in mass spectra of **7** and **8** to $[M + H]^+$ and $[M + Na]^+$ ions, respectively. The purity of the compounds was confirmed by elemental analyses. Circular dichroism (CD) spectra recorded for the aqueous solutions of nickel(II) and zinc(II) complexes of L-Pro-FTSC and D-Pro-FTSC (**1**, **2** and **7**, **8**) at physiological pH reveal that all of them are optically active and show Cotton effects (see Figure S1 and S2 in the Supporting Information). As expected, they are mirror images over the 230−350 nm region of the CD spectra, while their UV−vis spectra are identical.

X-ray Crystallography. The results of X-ray diffraction studies of **1**−**3**, **6** and **7** are shown in Figure S3 (see Supporting Information) and Figures 1–4. The complexes **1**−**3** and **6** crystallized in the noncentrosymmetric orthorhombic space group $P2_12_12_1$, while **7** in the noncentrosymmetric monoclinic space group $P2_1$. The proline-thiosemicarbazone hybrids L-Pro-FTSC, D-Pro-FTSC and/or dm-L-Pro-FTSC in **1**−**3** and **6**, **7** act as pentadentate doubly-deprotonated ligands binding to nickel(II), copper(II) or zinc(II) via pyridine nitrogen atom, imine nitrogen, thiolato S atom, tertiary proline nitrogen, and proline carboxylato oxygen atom. While in copper(II) and zinc(II) complexes **6** and **7** (Figures 3 and 4) the coordination number (CN) of the central metal ion is 5, and the coordination polyhedron can be described as a square-pyramid (τ = 0.09 and 0.07, respectively),[73] the CN of the nickel(II) in compounds **1**−**3** is increased to 6 by coordination of an adjacent Ni(L-Pro-FTSC−2H), Ni(D-Pro-FTSC−2H) or Ni(dm-L-Pro-FTSC−2H) complex via thiolato S atom, which acts as a bridging ligand between two nickel(II) ions associating the two monomeric complexes in a dimer (Figures S3, 1 and 2). One precedence of a related thiolato-bridged dimer with a central Ni(μ-S)$_2$Ni core, in which each nickel(II) atom is surrounded by O, N, S donor atoms of a tridentate doubly deprotonated 5-nitrobenzaldehyde 4N-methylthiosemicarbazone (H_2L), and two nitrogen atoms of a bipyridine coligand, characterized by X-ray diffraction, has been found in CSD data base.[74] Upon coordination of L-prolinate moiety to metal ion via the nitrogen atom, the latter, in addition to C12 (or C14 in **3** and **6**), becomes a chiral center. In contrast to the literature reports,[75] where in most cases the nitrogen atom adopts the same configuration as the asymmetric prolinate carbon (S_CS_N or R_CR_N), in complexes **1**−**3**, **6** and **7** the nitrogen and the asymmetric carbon of the proline moiety adopt opposite configurations by coordination to metal (S_CR_N or R_CS_N). Documented opposite configurations resulted from coordination to metal ion or protonation of the proline nitrogen atom are rare.[76] Of note is the formation of four five-membered chelate cycles upon coordination of the ligand to metal ion. Three of these are essentially planar, while the fourth prolinic moiety adopts a half-chair conformation.

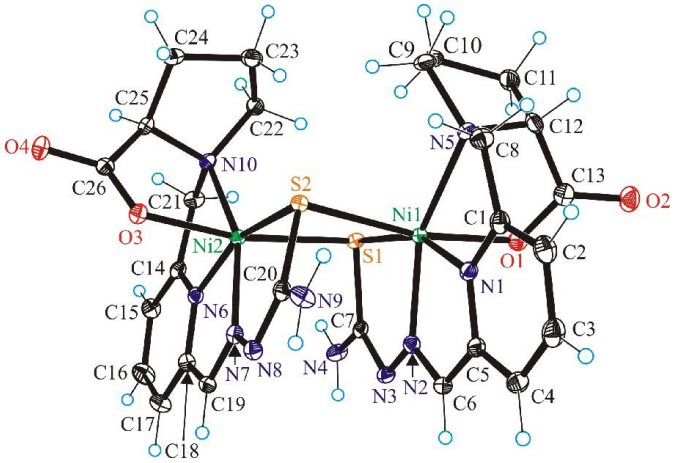

Figure 1. ORTEP view of **2** with thermal displacement ellipsoids drawn at the 50% probability level. Selected bond distances (Å) and bond angles (deg): Ni1−N1 1.9944(17), Ni1−N2 2.0515(17), Ni1−N5 2.2247(18), Ni1−S1 2.3946(5), Ni1−S2 2.4995(5), Ni1−O1 2.0766(15), N2−N3 1.363(2), C7−S1 1.762(2); N1−Ni1−N2 78.71(7), N1−Ni1−N5 78.08(7), N5−Ni1−O1 81.40(6), N1−Ni1−O1 87.41(6), N2−Ni1−O1 88.37(6), S1−Ni1−O1 96.00(4), S1−Ni1−S2 86.845(18), Ni1−S1−Ni2 92.065(18), Ni1−S2−Ni2 92.648(18), Ni2−N6 1.9894(17), Ni2−N7 2.0496(17), Ni2−N10 2.2107(16), Ni2−S2 2.4042(5), Ni2−S1 2.5321(6), Ni2−O3 2.0417(14), N7−N8 1.367(2), C20−S2 1.770(2); N6−Ni2−N7 78.83(7), N6−Ni2−N10 79.09(7), N10−Ni2−O3 81.55(6), N6−Ni2−O3 89.72(6), N7−Ni2−O3 89.52(6), S2−Ni2−O3 93.26(4), S1−Ni2−S2 85.905(18).

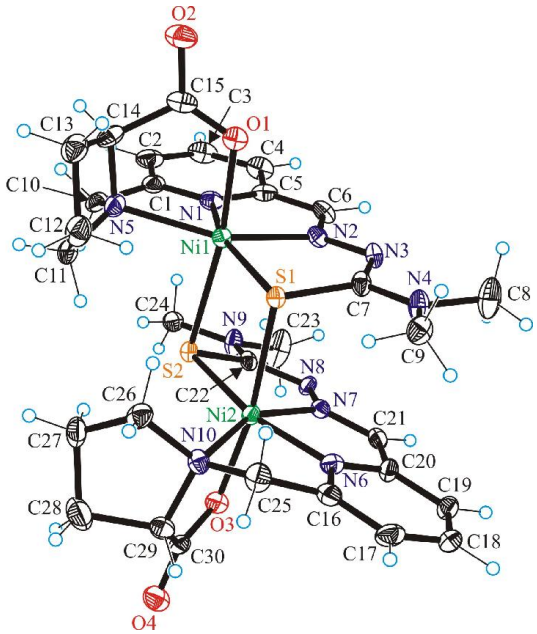

Figure 2. ORTEP view of **3** with thermal displacement ellipsoids drawn at the 50% probability level. Selected bond distances (Å) and bond angles (deg): Ni1−N1 1.975(3), Ni1−N2 2.027(3),

Ni1−N5 2.199(4), Ni1−S1 2.3896(11), Ni1−S2 2.5239(11), Ni1−O1 2.059(3), N2−N3 1.359(5), C7−S1 1.766(4); N1−Ni1−N2 79.10(14), N1−Ni1−N5 79.17(14), N5−Ni1−O1 80.98(13), N1−Ni1−O1 89.41(13), N2−Ni1−O1 89.49(13), S1−Ni1−O1 95.82(9), S1−Ni1−S2 86.12(4), Ni1−S1−Ni2 93.22(4), Ni1−S2−Ni2 93.86(4), Ni2−N6 1.989(3), Ni2−N7 2.038(3), Ni2−N10 2.198(3), Ni2−S2 2.3758(11), Ni2−S1 2.5360(11), Ni2−O3 2.032(3), N7−N8 1.355(5), C22−S2 1.767(4); N6−Ni2−N7 79.08(14), N6−Ni2−N10 79.01(14), N10−Ni2−O3 81.18(12), N6−Ni2−O3 91.80(13), N7−Ni2−O3 89.03(12), S2−Ni2−O3 90.76(9), S1−Ni2−S2 86.14(4).

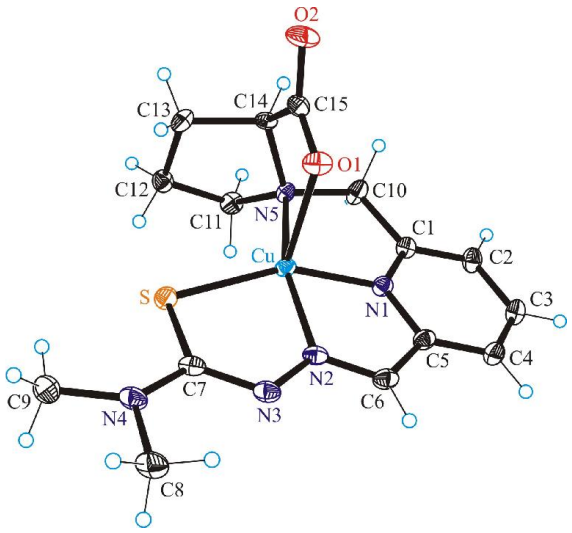

Figure 3. ORTEP view of **6** with thermal displacement ellipsoids drawn at the 50% probability level. Selected bond distances (Å) and bond angles (deg): Cu−N1 1.9335(11), Cu−N2 1.9887(11), Cu−S 2.2668(4), Cu−N5 2.1343(11), Cu−O1 2.1655(10), N2−N3 1.3511(15), C7−S 1.7636(13); N1−Cu−N2 80.36(5), N1−Cu−N5 81.75(4), N5−Cu−O1 79.14(4), N1−Cu−O1 94.63(4), N2−Cu−O1 106.20(4), S−Cu−O1 106.69(3).

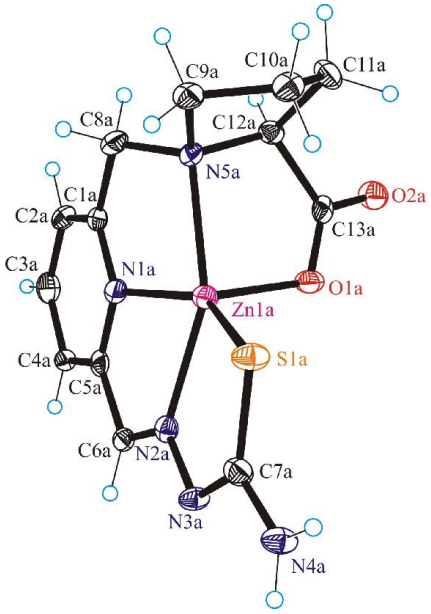

Figure 4. ORTEP view of **7** with thermal displacement ellipsoids drawn at the 50% probability level. Selected bond distances (Å) and bond angles (deg): Zn1a−N1a 2.066(3), Zn1a−N2a 2.140(3), Zn1a−S1a 2.2913(9), Zn1a−N5a 2.231(3), Zn1a−O1a 1.989(2), N2a−N3a 1.354(4), C7a−S1a 1.748(3); N1a−Zn1a−N2a 75.00(12), N1a−Zn1a−N5a 77.48(11), N5a−Zn1a−O1a 82.97(10), N1a−Zn1a−O1a 99.77(11), N2a−Zn1a−O1 105.14(10), S1a−Zn1a−O1a 107.26(8).

The complexes are involved in intermolecular hydrogen bonding interactions. In particular, the nitrogen atom N4 of one terminal amino group in the dimer **2** acts as a proton donor in hydrogen bonds to oxygen atoms O6 and O7 of the two co-crystallized methanol molecules (see Figure S4), while the nitrogen atom N9 of the second terminal amino group also forms two hydrogen bonds, one to carboxylato oxygen atom $O4^{i}$, and the second to $O8^{i}$ of the third co-crystallized methanol of the adjacent complex. The hydrazinic nitrogen N3, and carboxylate oxygens O1, O2 and O4 are proton acceptors in strong hydrogen bonds with $O8^{ii}$, $O5^{ii}$, $O6^{ii}$ and $O7^{i}$ of the neighboring methanol molecules, (atoms marked with i have been generated via symmetry transformation $x - 0.5, -y + 0.5, -z + 1$, while those with ii via symmetry transformation $-x + 0.5, -y + 1, z - 0.5$).

Dimethylation of the terminal amino group reduces strongly the involvement of complexes in intermolecular hydrogen bonding interactions, as can be seen in the crystal structures of **3** and **6**. Detail of H-bonding in **3** is not specified because of severe disorder of co-crystallized methanol

molecules in the crystal. The co-crystallized water molecule in **6** acts as a proton donor to carboxylato oxygen atom O2^{i} and thiolato atom S^{ii} forming two strong hydrogen bonds (Figure S5). Atoms marked with i have been generated via symmetry transformation $x + 1, y, z$, while those with ii via symmetry transformation $-x + 0.5, -y + 1, z + 0.5$.

The terminal amino group of both ctystallographically independent molecules A and B of the complex [Zn(L-Pro-FTSC)] (**7**) are involved as proton donors in hydrogen bonding to N3b (molecule B) and O2a^{i} (molecule A) and to N3a and O3b, respectively (Figure S6). The carboxylato oxygen atoms O2a and O2b act as proton acceptors in hydrogen bonds with O3a^{ii} and O3b^{ii}, which play a role of proton donors. Atoms marked with i, ii and iii have been generated via symmetry transformations $x + 1, y, z$, $-x, y + 0.5, -z + 1$ and $-x + 1, y + 0.5, -z + 1$, respectively.

Magnetic Properties. The magnetic properties of **1** have been investigated in the temperature range 2–300 K. At 300 K the $\chi_M T$ product (at 0.1 T) is 2.43 cm^3 K mol^{-1} and it increases when the temperature is lowered indicating the presence of ferromagnetic exchange interactions in the Ni_2 dimer (Figure 5). The room temperature magnitude of $\chi_M T$ imposes the upper limit of 2.2 on the g value. The $\chi_M T$ product increases continuously to reach a maximum of 3.16 cm^3 K mol^{-1} at about 20 K (Figure 5), and subsequently drops down to 2.01 cm^3 K mol^{-1} at 2 K as a result of ZFS or/and intermolecular interactions.

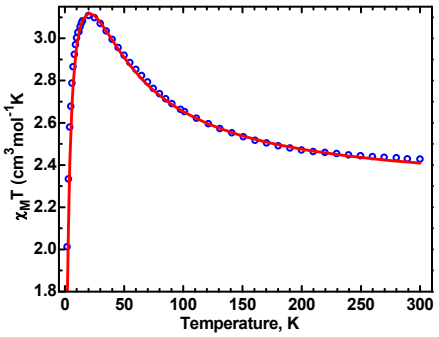

Figure 5. Plots of $\chi_M T$ and χ_M versus T for **2**. The red trace corresponds to the best fit with model parameters indicated in the text.

The fitting procedure led to J = +10.5(3) cm^{-1}, g = 2.13(2), $D_{(ZFS)}$ = +7.8 cm^{-1} (fixed), E = 2.2 cm^{-1} (fixed) zJ' = –0.29 cm^{-1} in reasonable agreement with the experimental data (R = 6 × 10^{-4}). When the restrictions on D and E are released, much better fit is possible even without the zJ' term, but the resulting D and E are in disagreement with the EPR data.

DFT calculations. "Broken-symmetry"[77] Density Functional Theory (DFT) calculations were performed using the software package ORCA[78] to get more insight into the exchange interactions. The X-ray coordinates were used in the calculations. The TZVPP function base was used for nickel and all coordinated atoms while VDZ functions were used for other atoms.[79] The B3LYP functional was employed.[80] In the "broken symmetry" procedure an SCF calculation is first performed on a molecule in the high-spin state (HS), which in our case is an S = 2 state. Next, a "broken symmetry" state (BS) is set up in which two unpaired electrons on one nickel(II) are spin-up and two electrons on another nickel(II) are spin-down and a second SCF calculation is performed. The exchange integral is then evaluated using: $J = -(E_{HS}-E_{BS})/(\langle S^2\rangle_{HS}-\langle S^2\rangle_{BS})$. J = 15 cm^{-1} was calculated, in a reasonable agreement with the result of the magnetic data fitting.

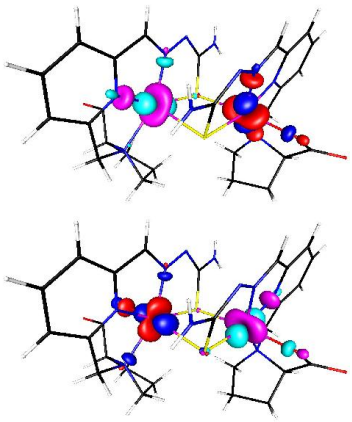

Figure 6. Two pairs of the magnetic orbitals of Ni(II) derived from the "broken symmetry" DFT calculations. Small overlap integrals (0.0065 and 0.0002 for the upper and lower pair, respectively) favor the ferromagnetic exchange.

Ferromagnetic interactions in the present dimer are reflected in weak overlap between the magnetic orbitals of the two nickel ions. The overlap integrals calculated from DFT for two pairs of the magnetic orbitals (Figure 6) are 0.0065 and 0.0002, which favors the ferromagnetic exchange. For comparison, in an antiferromagnetic dinuclear Ni(II) complex with $J = -78$ cm^{-1} (converted to the notation used in this paper), the overlap integrals of 0.042 and 0.075 were found in an analogous calculation.[81]

EPR Spectra. Well resolved high-field spectra were observed at frequencies over the range 50–420 GHz at 3 K - the lowest temperature that can be reached on our EPR instrument (Figure 7). At this temperature the spectra are expected to exhibit mainly transitions within the ground quintet state ($S = 2$). No resonances due to the excited $S = 1$ state were observed at higher temperatures as the spectra quality very quickly deteriorated with the temperature. The highest-field resonance in the 156 and 222 GHz spectra in Figure 7, which moves beyond the available magnetic field at higher frequencies, is the "Z" resonance in the $S = 2$ state.

The "giant spin" method requires that the coupled spin states are well separated from each other, which is not fulfilled in the present case where the exchange interactions are comparable to the zero-field splitting causing their mixing. Simulation of the powder spectra was thus not successful, but the observation of the high-field "Z" resonance over a wide range of frequencies (Figure S7) allowed determination of the D parameter in the $S = 2$ state of + 2.11 cm^{-1} and $g_z = 2.10$. If the zfs tensors of two ions were collinear, the D found above would imply that D on single ions is +6.33 cm^{-1}, neglecting the D_{12} term in eq 1.[64] However, there are complicating factors. The two nickel ions in our system are non-equivalent, thus their g matrices and the zero-field splitting tensors must be different. The molecular structure indicates that neither the g tensors of two ions nor their zfs tensors can be coaxial. In the EPR spectra of the dinuclear systems, the coupled g is observed and the zero-field splitting in the coupled states is affected by the zero-field splitting on the separate ions and by the anisotropic metal-metal interactions. The zero-field splitting of the coupled states depends not only on the $\{\boldsymbol{D}_1\}$, $\{\boldsymbol{D}_2\}$ and $\{\boldsymbol{D}_{12}\}$ component magnitudes but also on their orientation. This information is not available experimentally. Although DFT is not expected to provide correct magnitudes of the zfs parameters, calculations were performed in order to gain insight into the orientation of the $\{\boldsymbol{D}_1\}$ and $\{\boldsymbol{D}_2\}$ tensors and g

matrices of eq 1. The calculations, again performed by using ORCA, indicate that the "z" axis of the $\{\boldsymbol{D}_1\}$ tensor forms an angle of 26 deg with the $\{\boldsymbol{D}_2\}$ tensor "z" axis. With this arrangement it was found that D = +7.8 cm^{-1} and E = +2.2 cm^{-1} on each Ni ion are required to calculate the resonances marked with * and + in Figure 8 at right positions, assuming that the Ni ions are equivalent and neglecting the $\{D_{12}\}$ term in eq 1. It does not seem that we can extract more from our EPR data because of the lack of symmetry in the molecule. An additional aspect is that in the absence of the inversion center the antisymmetric exchange (Dzialoshiskii-Moriya interaction)[82] cannot be ruled out. High-field EPR studies on more symmetric systems were considerably more successful.[70]

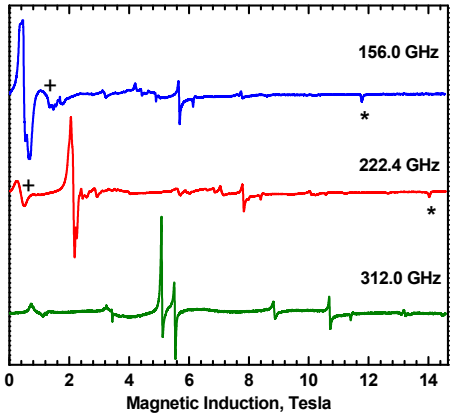

Figure 7. EPR spectra of **1** recorded at 3 K with the microwave frequencies as indicated. The resonance marked with * was identified as the |–2> ↔ |–1> transition and was used to determine D = +2.11 cm^{-1} and g_z = 2.10 within the "giant spin" formalism. That resonance would be frozen out at 3 K if D were negative. The line marked with + also appears to be a |–2> ↔ |–1> transition. When the frequency is lowered below 222 GHz, that transition moves to a higher field showing that the M_S levels involved are split in zero magnetic field by slightly more than 7.41 cm^{-1} (corresponding to the 222.4 GHz quantum energy). The E parameter of 0.52 cm^{-1} could be estimated.

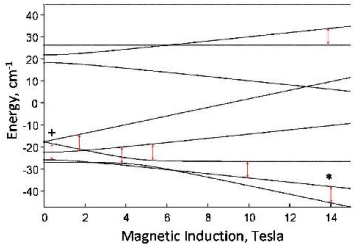

Figure 8. Energy levels calculated using the spin Hamiltonian (4) with $D_1 = D_2 = 7.8$ cm^{-1}, $E_1 = E_2 = 2.2$ cm^{-1}, $J = 11$ cm^{-1} and $g_z = 2.10$. The magnetic field is along the Z axis of the coupled system, that is along the bisector of the Z_1 and Z_2 axes of the Ni(II) ions. Transitions expected at 222.4 GHz are shown as vertical purple lines. * and + mark the same transitions as in Figure 7.

Solution Chemistry

Lipophilicity. The hydro-lipophilic character of dm-L-Pro-FTSC, its nickel(II) and copper(II) complexes **3** and **6**, as well as of both zinc(II) complexes of L-Pro-FTSC and D-Pro-FTSC (**7** and **8**) was studied at pH 7.4 via the partitioning between *n*-octanol and water. The data are summarized in Table S1. The enantiomers of the zinc(II) complexes of Pro-FTSC have similar log$D_{7.4}$ values (L: −1.41(9); D: −1.56(5)) indicating rather hydrophilic character. However, they are slightly more lipophilic than the ligands alone (log$D_{7.4}$ < −1.7).[49]

The nickel(II) complexes with L-Pro-FTSC and D-Pro-FTSC (**1** and **2**) were found to be very hydrophilic and practically no metal complex could be detected in the organic phase after partitioning. Therefore, only a threshold limit could be estimated for their distribution coefficients (log$D_{7.4}$ < −1.7) as in case of the ligands alone.[49] The dimethyl derivatives as expected were still hydrophilic, but appreciably more lipophilic than nonmethylated compounds.

Proton Dissociation Processes of the Ligand L-Pro-FTSC. pK_a values of L-Pro-FTSC (see Chart 1) were determined in aqueous solution by the combined approach of pH-potentiometric, UV–vis and ^{1}H NMR titrations in our previous work[49] and data obtained here were found to be identical with them. Although, this organic compound consists of four dissociable protons (COOH, $N_{Pro}H^+$, $N_{pyridine}H^+$ and $N_{hydrazinic}H$) only three pK_a values can be determined in the

studied pH-range. pK_1 (1.86) most probably belongs to the deprotonation of the COOH moiety (partly overlapped with the deprotonation of $N_{pyridine}H^+$) and pK_2 (8.78) and pK_3 (11.08) to $N_{Pro}H^+$ and the hydrazinic-NH functional groups, respectively. It is noteworthy that the ligand is mainly present in its neutral form at pH 7.4 adopting a zwitterionic structure, which results in excellent water-solubility and a fairly hydrophilic character.[49]

Complex Formation of L-Pro-FTSC with Zinc(II) and Nickel(II) in Aqueous Solution. Complex equilibria in water were investigated by pH-potentiometry in all cases and stoichiometries and cumulative stability constants of the metal complexes furnishing the best fits to the experimental data are listed in Table 2. The recorded titration curves indicate that L-Pro-FTSC is an efficient metal-ion chelator in a wide pH range for nickel(II) and zinc(II) ions. Representative titration curves (Figure 9) reveal that complex formation processes start at lowest pH in the case of nickel(II), while curves registered in the presence of zinc(II) are superimposed with that of the free ligand up to pH ~3.5. Fairly simple equilibrium model was obtained for all systems as formation of mono-ligand complexes ($[MLH]^+$, [ML] and $[MLH_{-1}]^-$) is the most probable (Table 2). In the protonated complexes $[MLH]^+$, the proton can presumably be attributed to the non-coordinating hydrazinic N^2 atom, while [ML] contains the completely deprotonated ligand. pK values of complexes $[MLH]^+$ are significantly lower than pK_2 ($N_{Pro}H^+$) and pK_3 (hydrazinic-NH) of the ligand in all cases, which strongly suggests the involvement of the Pro nitrogen into the coordination beside the thiosemicarbazide moiety in the complexes [ML]. Species $[MLH_{-1}]^-$ are regarded as mixed hydroxido complexes, i.e. $[ML(OH)]^-$.

Table 2. Cumulative (logβ ($M_pL_qH_r$)) and Derived Stability Constants of the Nickel(II)−, Copper(II)− and Zinc(II)− L-Pro-FTSC complexes[a] [T = 298 K and I = 0.10 M (KCl)]

	logβ $[MLH]^+$	Logβ [ML]	logβ $[MLH_{-1}]^-$	pK $[MLH]^+$	pM[b]
nickel(II)	20.73(2)	15.78(3)	5.04(4)	4.95[e]	11.7
copper(II)[c]	24.03	21.64	9.59	2.39	17.5
zinc(II)	18.28(3)	13.31(2)	−	4.97[d]	9.2

[a]The numbers in parentheses are standard deviations of the quoted logβ values determined by pH-potentiometry. Proton dissociation constants of the ligand: pK_1 =

1.86, pK_2 = 8.78 and pK_3 = 11.08 taken from reference 49. [b]pM = −log[M] at pH 7.40; c_L/c_M = 10; c_M = 0.001 mM. [c]Data are taken from ref. 49. [d]pK = 4.98(1) calculated from the ^{1}H NMR δ values of the CH=N protons of the bound ligand.

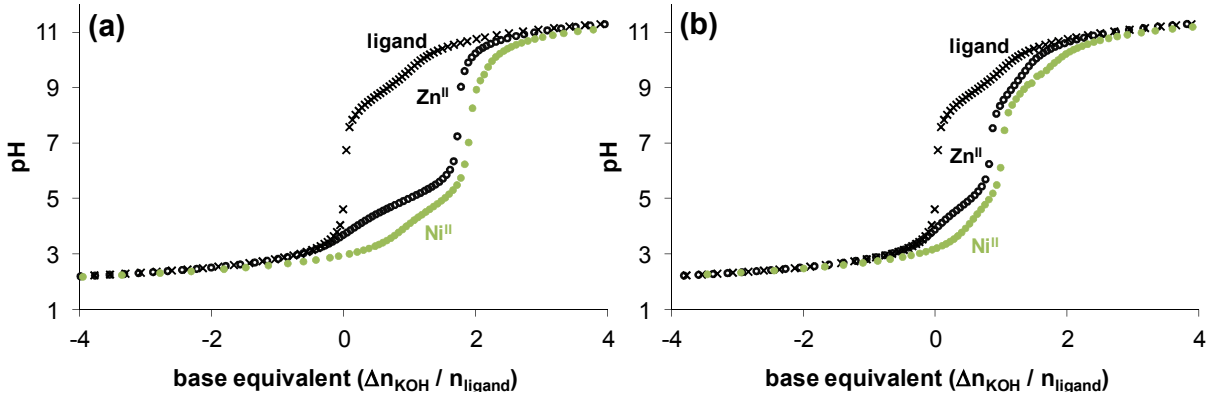

Figure 9. Representative pH-potentiometric titration curves for ligand L-Pro-FTSC (×), zinc(II)– ligand (○) and nickel(II)– ligand (●) systems [c_L = 0.0019 M; M:L = 1:1.1 (a) and 1:2.3 (b); T = 298 K and I = 0.10 M (KCl) in water]. *Negative base equivalent values mean an excess amount of acid.*

Direct comparison of the overall stability constants (logβ) represents well the stability rank order of the metal complexes formed with the studied ligand: nickel(II) > zinc(II). It is noteworthy that copper(II) forms complexes with L-Pro-FTSC with unquestionably higher stability compared with these bivalent metal ions. First of all pM values have been computed in order to compare the extent of complex formation at physiological pH (Table 2). The higher pM value represents stronger chelating ability. pM values calculated show that the ligand effectiveness is increased in the following order: zinc(II) < nickel(II) < copper(II). Additionally the distribution of the mono complexes of zinc(II) and nickel(II) was calculated based on the determined stability constants at physiological pH at various total concentrations and depicted in Figure 10. Complexes [ML] predominate at this pH in all cases and as it is expected the partial dissociation resulting in free ligand and metal ion is more pronounced with decreasing total concentrations. Nickel(II) is able to preserve the original entity more efficiently owing to the higher stability of its complex, however even in the case of zinc(II) the decomposition of [ZnL] is only 8% at 1 μM concentration at pH 7.4.

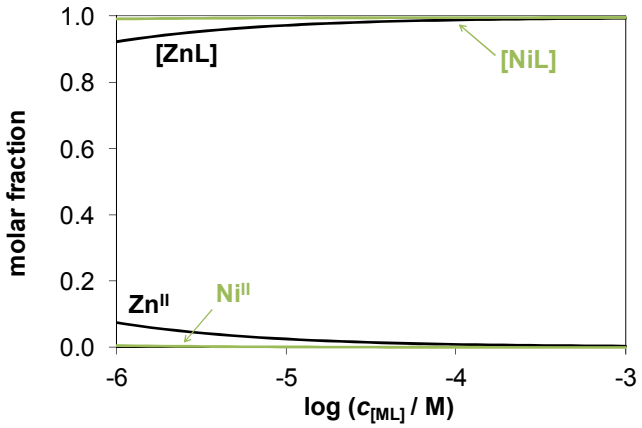

Figure 10. Concentration distribution curves for the metal(II) − L-Pro-FTSC systems at various total concentrations of the [ML] complexes at pH 7.40 [T = 298 K and I = 0.10 M (KCl)].

In order to confirm the speciation obtained by pH-potentiometry for the zinc(II) − L-Pro-FTSC system ^{1}H NMR spectroscopic measurements were applied. Slow ligand-exchange processes are seen with respect to the NMR time scale as the chemical shifts of the protons of the free and Zn-bound ligand are observed separately (Figures 11 and S8).

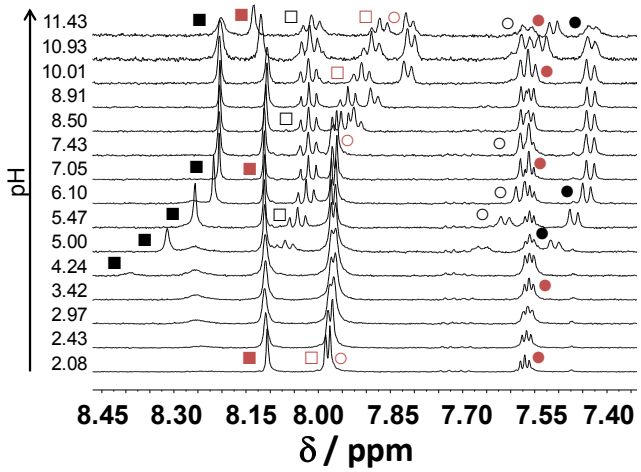

Figure 11. Low-field region of the ^{1}H NMR spectra recorded for the zinc(II) − L-Pro-FTSC system at the indicated pH values. Black symbols are shown for the bound ligand and red symbols for the nonbound ligand: ●: $CH_{Ar}(6)$; ○: $CH_{Ar}(4)$; □: $CH_{Ar}(5)$; ■: CH=N; [c_L = 1.0 mM; Zn:L = 1:2; T = 298 K and I = 0.10 M (KCl); 10% D_2O].

Peaks belonging only to the nonbound ligand are seen at pH < ~4 and a new set of signals appears additionally with increasing pH, which belongs, most probably, to the protonated complex $[ZnLH]^+$. Its deprotonation is accompanied by significant electronic shielding effects, namely an upfield shift of the peaks in the low-field region of the spectra. p*K* value of $[ZnLH]^+$ calculated on the basis of the change of the signals of the CH=N protons of the bound ligand (Table 3) is in good agreement with that obtained from the pH-metric titration data. The peaks of species [ZnL] have constant positions at pH 7 − 11.5, which strongly suggests that the formation of a mixed-hydroxido complex $[ZnL(OH)]^-$ is not probable in this pH range. The integrated areas of the corresponding CH=N peaks of the bound and nonbound ligand could be calculated and converted to molar fractions, which were also computed under the same conditions based on the stability constants obtained by pH-potentiometry (Figure 12). The strong correlation between the data of the two independent methods supports the accuracy of the stability constants determined.

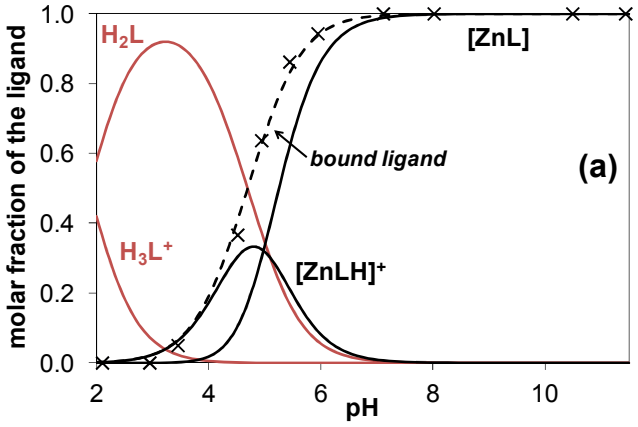

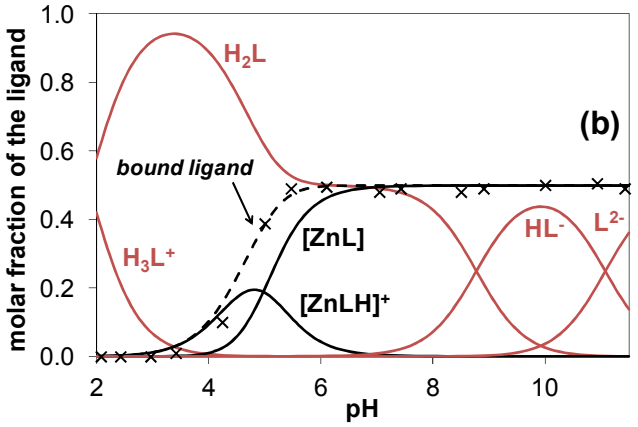

Figure 12. Concentration distribution curves of the zinc(II) − L-Pro-FTSC system at 1:1 (a) and 1:2 (b) metal-to-ligand ratios obtained with the help of the stability constants (solid lines) together with the summed molar fraction of the bound ligand calculated (dashed line) and estimated from the integrated area of the signals of the CH=N proton (×) [c_L = 1.0 mM; T = 298 K and I = 0.10 M (KCl)].

In the case of the outstanding high stability [CuL] complex of L-Pro-FTSC the coordination of the COO^- and proline-N functionalities of the Pro moiety in addition to the (N_{pyr},N,S^-) donor set of thiosemicarbazide moiety could be proved both in solution and in solid phase in our previous work.[49] The relatively high stability of the [ZnL] complex, which predominates at neutral pH even at micromolar concentrations, supports a similar binding pattern in solution. Moreover, the pentadentate (N_{pyr},N,S^-,COO^-,N_{Pro}) coordination mode of L-Pro-FTSC to zinc(II) was also confirmed by single-crystal X-ray diffraction (Figure 4).

The pentadentate binding of the ligand was also found in the case of nickel(II) in the solid phase, although the thiosemicarbazone sulfur atom acts as a bridging ligand in the dinuclear species crystallized out from the solution (Figures S1 and 1, 2). The pH-potentiometric titration curves for the nickel(II) − L-Pro-FTSC system could be fitted by the assumption of monomer complexes (Table 2), however this method has limitations in distinguishing between the formation of mononuclear and dinuclear species with the same metal-to-ligand ratio; therefore clarifying the actual coordination mode of the nickel(II) complexes in solution is more difficult. In order to confirm the speciation model obtained by pH-potentiometry and to get an insight into the geometry of the complexes UV–vis spectrophotometric and ^{1}H NMR measurements were performed. According to the electronic absorption spectra (Figure 13), formation of octahedral nickel(II) complexes is probable with this ligand in the measured pH range due to the lack of the characteristic bands of the square-planar complexes in the visible region. Additionally, the pH-dependent ^{1}H NMR spectra (Figure 14a) represent broad signals accompanying the formation of the nickel(II) complexes (Figure 14b), which strongly suggests the presence of high-spin, paramagnetic species with octahedral geometry in solution.

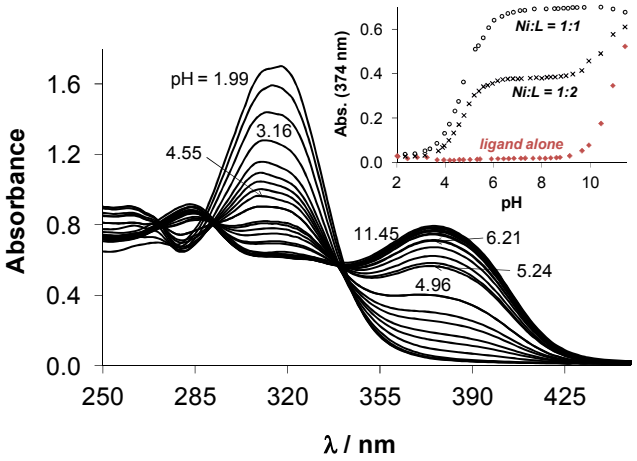

Figure 13. UV–vis spectra recorded for the nickel(II) − L-Pro-FTSC system at various pH values; [c_L = 0.160 mM; Ni:L = 1:1; l = 0.5 cm; T = 298 K and I = 0.10 M (KCl)]. *Inset shows the pH-dependence of the absorbance values at 374 nm for the same system (○) together with those recorded for the ligand alone (♦) and at 1:2 metal-to-ligand ratio (×) for comparison.*

On the other hand, UV–vis spectra at 1:1 metal-to-ligand ratio were measured in a wide concentration range (1 μM – 0.8 mM) at pH 7.4. A clear linear correlation was found between the absorbance and concentration (Figure S9) representing the unchanged molar absorptivity (ε), thus unchanged species (ratio) in the studied concentration range. Dilution generally can shift the monomer/dimer equilibrium to the direction of dissociation affecting the ε values as the ratio of the mononuclear and dinuclear species would change. Thus, the formation of only monomer [NiL] species in solution is more probable due to the constant ε values.

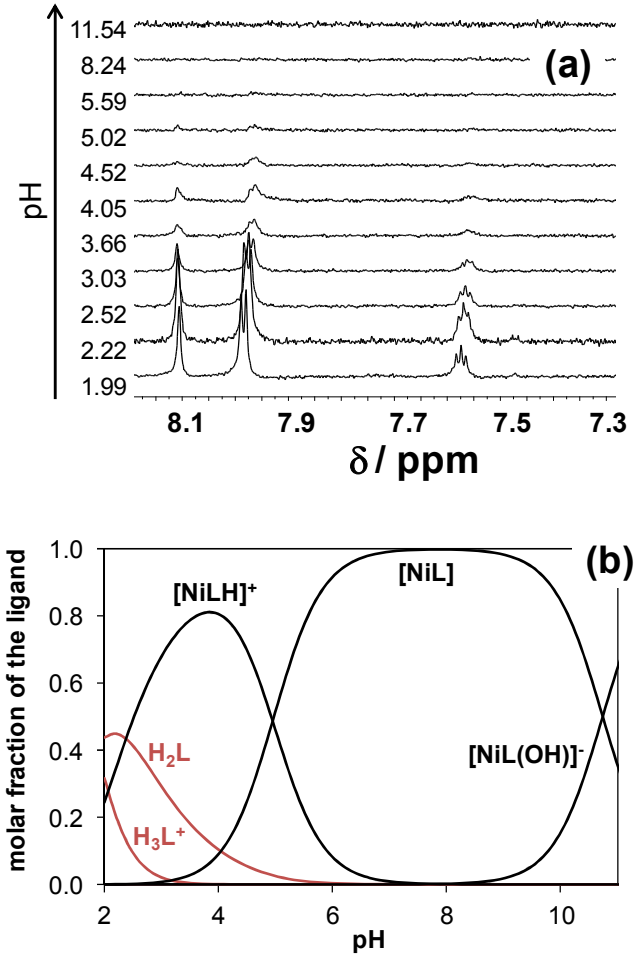

Figure 14. Low-field region of the ^{1}H NMR spectra recorded for the nickel(II) − L-Pro-FTSC system at the indicated pH values (a) [c_L = 1.0 mM; Ni:L = 1:1; T = 298 K and I = 0.10 M (KCl); 10% D_2O] and concentration distribution curves for the same system (b).

Stability of the Zinc(II) Complex of L-Pro-FTSC in Minimum Essential Medium (MEM) and its Interaction with HSA. MEM is usually used for the in vitro cytotoxicity studies and contains various amino acids which can potentially compete for the metal ion with the original ligand. To assess the stability of the [ZnL] complex of L-Pro-FTSC in the MEM, ^{1}H NMR spectra of the complex were measured in this medium and in aqueous solution at pH 7.40 for comparison (Figure S10). The peaks of [ZnL] in MEM seem to remain unchanged compared to those detected in water and no free ligand is liberated due to a possible ligand displacement by

the amino acids. This provides strong evidence that the complex is stable in MEM. (Since nickel(II) complexes possess logβ values by two orders of magnitude higher than those of zinc(II), no ligand displacement reactions are expected in MEM.)

Competition reaction for the zinc(II) ion between L-Pro-FTSC and the most abundant blood serum protein, HSA was followed by ^{1}H NMR spectroscopy. HSA serves as a transport vehicle for a wide variety of endogenous species such as copper(II) and zinc(II) ions and exogenous compounds and various pharmaceuticals. At the proposed Zn-binding site of HSA (*Multi-Metal Binding Site*) two His N atoms, an Asn carboxylate, an Asp carboxylate, and a water molecule are coordinated to the metal ion.[83] The conditional binding constants of HSA for zinc(II) under physiological conditions are given in the literature as log$K$' ~7.1–7.9.[84] The ^{1}H NMR spectrum recorded in the presence of HSA (Figure 15) clearly shows the partial displacement of L-Pro-FTSC by the protein (~30%) under the given condition. Beside HSA, human serum transferrin (Tf) has also zinc(II) binding ability at the iron-binding sites;[85] however, the concentration of Tf is approximately 17 times lower compared to that of HSA. Concentration distribution curves were computed for the zinc(II) complex of L-Pro-FTSC in the presence of these serum proteins at pH 7.4 at various total concentrations taking into consideration the stability constants of the zinc(II) complexes of the ligand, HSA and Tf (Figure S11a). These calculations reveal that ~30% of zinc(II) is bound to HSA at mM concentrations (as the ^{1}H NMR spectrum also showed in Figure 15), while more than 80% at 10 μM. The role of Tf seems to be almost negligible in this concentration range. Based on similar computational modelings, it can be concluded that the higher stability nickel(II) and copper(II) complexes are able to preserve their original composition stronger in the presence of the serum proteins (Figure S11b,c).[86]

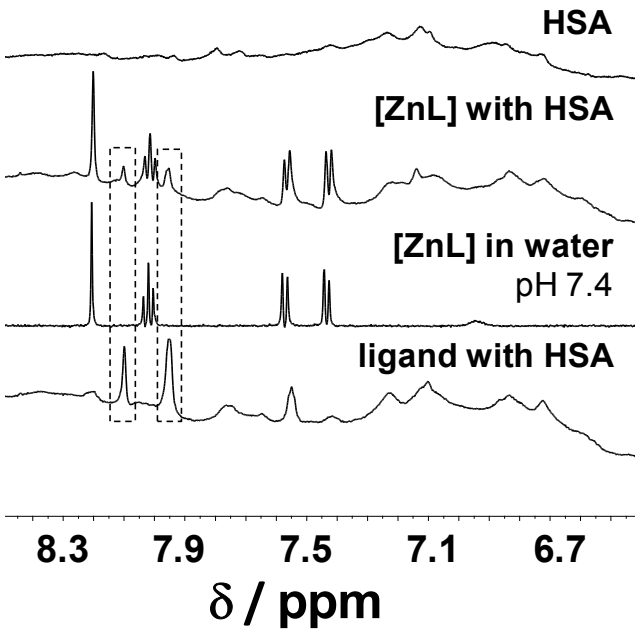

Figure 15. Low-field region of the ^{1}H NMR spectra of HSA, complex [ZnL] of L-Pro-FTSC with HSA and in HEPES buffer (20 mM) at pH 7.40 and for L-Pro-FTSC with HSA [c_L = 1.0 mM; c_{HSA} = 0.63 mM; T = 298 K and I = 0.10 M (KCl); 10% D_2O]. Peaks framed up correspond exclusively to the nonbound ligand.

Cytotoxicity in Cancer Cell Lines. The antiproliferative activity of the investigated compounds (**1**–**3** and **6**–**8**) was evaluated for 48 h of continuous drug action, using colorimetric MTT assay. The study was performed in several human neoplastic cell lines (HeLa, FemX, A549, MDA-MB-453), and one human fetal lung fibroblast cell line (MRC-5), which was used as a noncancerous model for the *in vitro* toxicity evaluation. The obtained cytotoxicity results for the nonmethylated metal-free hybrids L-Pro-FTSC and D-Pro-FTSC and their nickel(II), copper(II) and zinc(II) complexes revealed that all compounds possessed poor activity (IC_{50} > 300 μM) against all cell lines used (HeLa, FemX, MDA-MB-453). Complex formation of the FTSC-proline hybrids with nickel(II), copper(II) and zinc(II) (**1**, **2**, **4**, **7** and **8**) does not enhance antiproliferative effects *in vitro*.

We further investigated the antiproliferative activity of the dm-L-Pro-FTSC hybrid and its copper(II) and nickel(II) complexes. The results shown in Table 3 indicate that dimethylation improves the cytotoxicity of the hybrid (IC_{50}(dm-L-Pro-FTSC) < IC_{50}(D-Pro-FTSC and L-Pro-FTSC). Complex formation of dm-L-Pro-FTSC with copper(II) (complex [Cu(dm-L-Pro-FTSC)] (**6**)) significantly increases cytotoxicity towards HeLa and MRC5 cell lines compared to dm-L-Pro-FTSC hybrid alone (IC_{50} values 98.3 ± 5.5 and 69.4 ± 4.7 μM, compared to 224.6 ± 6.4 and 178.4 ± 1.5 μM, respectively). These results, showing that dimethylation has a favourable impact on cytotoxicity, are in accordance with the previously reported studies.[54,87]

Table 3. Results of MTT assay presented as IC_{50} (μM) values after 48 h incubation time. IC_{50} values were calculated as mean values obtained from two to three independent experiments and quoted with their standard deviations.

	IC_{50}/μM - (mean ± SD)		
Compound/cell line	HeLa	A549	MRC5
L-Pro-FTSC	> 300	> 300	> 300
dm-L-Pro-FTSC	224.6 ± 6.4	204.3 ± 4.8	178.4 ± 1.5
$[Ni(dm\text{-}L\text{-}Pro\text{-}FTSC{-}2H)]_2$ (**3**)	> 300	> 300	> 300
[Cu(dm-L-Pro-FTSC−2H)] (**6**)	98.3 ± 5.5	176.8 ± 1.7	69.4 ± 4.7
CDDP[a]	7.8 ± 2.3	17.2 ± 0.7	30.3 ± 3.0

The sign > (in front of the maximum value of the concentration) indicates that IC_{50} value is not reached in the examined range of concentrations. Compounds contain co-crystallized solvent (see Experimental section).

[a] taken from ref. [88]

Ribonucleotide reductase inhibition capacity. The reduction of the tyrosyl radical content in human R2 RNR protein by L-Pro-FTSC and dm-L-Pro-FTSC hybrids, and complexes **4**, **6**, and **7** was monitored by EPR spectroscopy. The hR2 protein exhibits an EPR spectrum that arises from

the tyrosyl radical associated with enzyme activity (Figure 16b inset).[89] It was observed that in the non-reducing conditions, the compounds are not active in tyrosyl radical destruction (Figure 16a). Moreover, complex **4** caused a small increase in tyrosyl radical content, an effect which was previously observed when mouse R2 protein (mR2) was incubated with only DTT.[24,90] An increase in radical content is caused by the continued radical reconstitution process which requires the presence of oxygen. This result indicates that in the absence of a reductant, complex **4** may have a protective role for the tyrosyl radical in hR2.

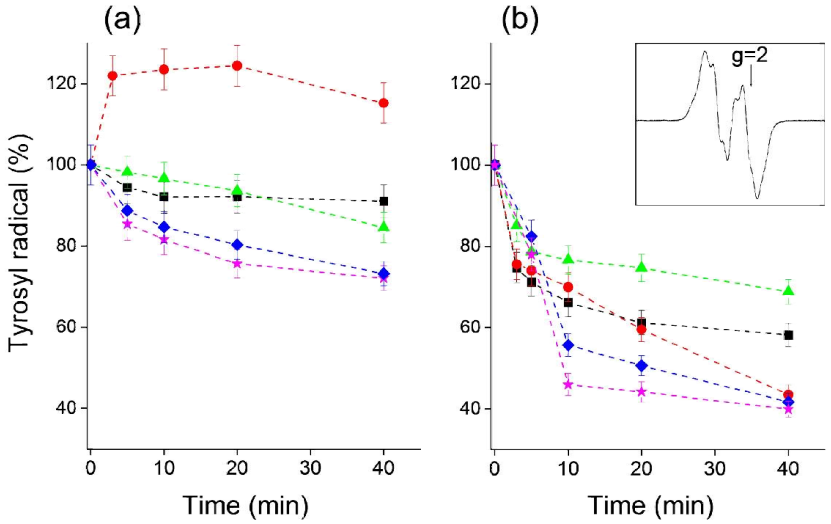

Figure 16. Tyrosyl radical reduction in human R2 RNR protein in (a) absence, and (b) presence of the external reductant DTT, by ligands L-ProFTSC (black trace), and dm-L-Pro-FTSC (blue trace), and complexes **4** (red trace), **6** (magenta trace), and **7** (green trace). The samples contained 20 µM hR2 protein in Tris buffer, pH 7.60 / 100 mM KCl / 5% glycerol, 20 µM compound (1% (w/w) DMSO/H_2O) and 2 mM DTT (only b). Error bars are standard deviation from two independent experiments. Inset shows EPR spectrum of the tyrosyl radical in hR2 RNR protein at 20 K. Experimental conditions are given in the Experimental section.

In the presence of an external reductant (DTT), all compounds showed appreciable radical destruction capacity compared to the nonreducing conditions (Figure 16b). The reduction by complex **4** was more efficient than by the ligand L-Pro-FTSC alone, indicating that the presence of the redox active copper(II) ion influences the inhibitory potential. Inhibition by complex **7** did not change markedly upon addition of DTT, as this compound contains zinc(II) which is redox inactive. Among the five tested compounds, dm-L-Pro-FTSC and complex **6** proved to be the best inhibitors, **6** being slightly more potent due to the presence of the copper(II) ion. The difference in the extent of the radical reduction observed between ligands L-Pro-FTSC and dm-L-Pro-FTSC (and their corresponding copper(II) complexes, **4** and **6**) indicates that the presence of two methyl groups increases the potency of the ligand.

It is interesting to compare these compounds with Triapine which is an analog of 2-formylpyrine thiosemicarbazone. Triapine was shown to be a good mR2[24] and hR2[25] inhibitor. In both proteins, Triapine exhibited 70% radical reduction after 20 min in the absence of the reductant, and reduced the radical completely after 5 min in the presence of DTT. This suggests that the proline moiety decreases the inhibitory potential of the ligand.

Conclusion

Nickel(II) and zinc(II) complexes with chiral proline-thiosemicarbazone hybrids L- and D-Pro-FTSC have been synthesized and characterized by standard analytical methods and in the case of complexes **1**–**3** also by single crystal X-ray diffraction. The temperature dependence of magnetic susceptibility, high-field EPR spectra and DFT calculations indicate ferromagnetic interaction between paramagnetic Ni(II) ions in **1** with the total spin ground state S_T = 2. As these complexes possess excellent water solubility, the solution speciation of nickel(II) and zinc(II) complexes of L-Pro-FTSC has been characterized in pure aqueous solution via a combined approach using pH-potentiometry, ^{1}H NMR spectroscopy and UV–vis spectrophotometry. Stability of the species formed is compared to that of copper(II) complexes. Exclusive formation

of the mono-ligand complexes such as $[MLH]^+$, [ML] and $[ML(OH)]^-$ was detected. L-Pro-FTSC was found to act as a pentadentate ligand in solution coordinating the metal ions via the (N_{pyr},N,S^-,COO^-,N_{Pro}) donor atoms. This binding mode was confirmed by X-ray crystallography in the case of the [ZnL] complex. On the other hand, nickel(II) forms a dinuclear complex with a central $Ni(\mu\text{-}S)_2Ni$ core in solid state and the two metal ions are chelated by the (N_{pyr},N,S^-,COO^-,N_{Pro}) donor set; however, the presence of monomeric species in solution is somewhat more probable. In the protonated $[MLH]^+$ complexes the pentadenate (N_{pyr},N,S,COO^-,N_{Pro}) binding mode with a protonated noncoordinating hydrazine N^2 atom is suggested. Based on the determined stability constants the effectiveness of L-Pro-FTSC to chelate the metal ions is in the rank order zinc(II) < nickel(II) < copper(II). The predominant species at pH = 7.4 are [ML] complexes in all cases. Complexes of zinc(II), nickel(II) and copper(II) possess so high stability that they remain intact during dilution at physiological pH in the biologically relevant micromolar concentration range. Additionally, [ZnL] remains unaltered in MEM, while partial displacement of L-Pro-FTSC by HSA in the serum is probable, especially at lower concentrations of the complex. The compound L-Pro-FTSC was N-terminally dimethylated and the structures of its nickel(II) and copper(II) complexes were determined by X-ray crystallography. Compounds prepared in this work were tested for antiproliferative activity in different human cancer cell lines. It was shown that dimethylation of terminal aminogroup in L- and D-Pro-FTSC resulted in antiproliferative activity of the hybrids. Coordination to copper(II) further enhances the cytotoxicity of the dimethylated hybrid. hR2 RNR inhibition capacity of selected compounds was also assayed. It was found that they are not active in tyrosyl radical destruction under nonreducing conditions, while they exhibit much stronger radical quenching capacity in the presence of the applied reductant DTT. The N-terminal dimethylation resulted in higher inhibitory potential of the ligand and its copper(II) complex. Further increase of the lipophilicity of proline-thiosemicarbazone hybrids via esterification of the proline moiety, and attachment of naphthyl, trimethylsilyl groups at the terminal nitrogen atom, which are underway in our laboratory, should result in more effective antiproliferative agents suitable for further development as potential anticancer drugs.

Supporting Information Available:

This material is available free of charge via the Internet at http://pubs.acs.org.

Author Information

Corresponding Author

* E-mail: enyedy@chem.u-szeged.hu (E.A.E.); vladimir.arion@univie.ac.at (V.B.A.).

Acknowledgments. This work was supported by the Hungarian Research Foundation OTKA project PD103905. This research was realized in the frames of TÁMOP 4.2.4. A/2-11-1-2012-0001 „National Excellence Program – Elaborating and operating an inland student and researcher personal support system". A.P.-B. and M.M. acknowledge the financial support from Serbian Ministry for Education, Science and Technological Development (grant III41005). The high-field EPR spectra were recorded at the NHMFL, which is funded by the NSF through the Cooperative Agreement No. DMR-1157490, the State of Florida, and the DOE. We thank Dr. Ghenadie Novitchi for helpful discussion of magnetic properties of **1**.

References

(1) Yu, Y.; Kalinowski, D. S.; Kovacevic, Z.; Siafakas, A. R.; Jansson, P. J.; Stefani, C.; Lovejoy, D. B.; Sharpe, P. C.; Bernhardt, P. V.; Richardson, D. R. *J. Med. Chem.* **2009**, *52*, 5271−5294.

(2) Casas, J. S.; Garcia-Tasende, M. S.; Sordo, J. *Coord. Chem. Rev.* **2000**, *209*, 197−261.

(3) Beraldo, H.; Gambino, D. *Mini-Rev. Med. Chem.* **2004**, *4*, 31−39.

(4) Rodríguez-Argüelles, M. C.; López-Silva, C.; Sanmartín, J.; Pelegatti, P.; Zani, F. *J. Inorg. Chem.* **2005**, *99*, 2231−2239.

(5) Quenelle, D. C.; Keith, K. H.; Kern, E. R. *Antiviral Res.* **2006**, *71*, 24−30.

(6) Joseph, M.; Suni, V.; Kurup, M. R. P.; Nethaji, M.; Kishore, A.; Bhat, S. G. *Polyhedron*, **2004**, *23*, 3069−3080.

(7) Brockman, R. W.; Thomson, J. R.; Bell, M. J.; Skipper, H. E. *Cancer Res.* **1956**, *16*, 167−170.

(8) Wadler, S.; Makower, D.; Clairmont, C.; Lambert, P.; Fehn, K.; Sznol, M. J. *J. Clin. Oncol.* **2004**, *22*, 1553−1563.

(9) Kolesar, J.; Brundage, R. C.; Pomplun, M.; Alberti, D.; Holen, K.; Traynor, A.; Ivy, P.; Wilding, G. *Cancer Chemother. Pharmacol.* **2011**, *67*, 393−400.

(10) Nutting, C. M.; van Herpen, C. M. L.; Miah, A. B.; Bhide, S. A.; Machiels, J.-P.; Buter, J.; Kelly, C.; de Raucourt, D.; Harrington, K. J. *Ann. Oncol.* **2009**, *20*, 1275−1279.

(11) Giles, F. J.; Fracasso, P. M.; Kantarjian, H. M.; Cortes, J. E.; Brown, R. A.; Verstovsek, S.; Alvarado, Y.; Thomas, D. A.; Faderl, S.; Garcia-Manero, G.; Wright, L. P.; Samson, T.; Cahile, A.; Lambert, P.; Plunkett, W.; Sznol, M.; DiPersio, J. F.; Gandhi, V. *Leuk. Res.* **2003**, *27*, 1077−1083.

(12) Karp, J. E.; Giles, F. S.; Gojo, I.; Morris, L.; Greer, J.; Johnson, B.; Thein, M.; Sznol, M. *Leuk. Res.***2008**, *32*, 71−77.

(13) Zeidner, J. F.; Karp, J. E.; Blackford, A. L.; Douglas Smith, B.; Gojo, I.; Gore, S. D.; Levis, M. J.; Carraway, H. E.; Greer, J. M.; Percy Ivy, S.; Pratz, K. W.; McDevitt, M. A. *Heamatologica* **2014**, *99*, 672−678.

(14) Mackenzie, M. J.; Saltman, D.; Hirte, H.; Low, J.; Johnson, C.; Pond, G.; Moore, M. J. *Invest. New Drugs* **2007**, *25*, 553−558.

(15) Attia, S.; Kolesar, J.; Mahoney, M. R.; Pitot, H. C.; Laheru, D.; Heun, J.; Huang, W.; Eickhoff, J.; Erlichman, C.; Holen, K. D. *Invest. New Drugs* **2008**, *26*, 396−379.

(16) Traynor, A. M.; Lee, J.-W.; Bayer, G. K.; Tate, J. M.; Thomas, S. P.; Mazurczak, M.; Graham, D. L.; Kolesar, J. M.; Schiller, J. H. *Invest. New Drugs* **2010**, *28*, 91−97.

(17) Knox, J. J.; Hotte, S. J.; Kollmannsberger, C.; Winquist, E.; Fisher, B.; Eisenhauer, E. A. *Invest. New Drugs* **2007**, *25*, 472−477.

(18) Moore, E. C.; Zedeck, M. S.; Agrawal, K. C.; Sartorelli, A. C. *Biochemistry* **1970**, *9*, 4492−4498.

(19) French, F. A.; Blanz, E. J.; Shaddix, S. C.; Brockman, R. W. *J. Med. Chem.* **1974**, *17*, 172−181.

(20) Kolberg, M.; Strand, K. R.; Graff, P.; Andersson, K. K. *Biochim. Biophys. Acta* **2004**, *1699*, 1−34.

(21) Green, D. A.; Antholine, W. E.; Wong, S. J.; Richardson, D. R.; Chitambar, C. R. *Clin. Cancer Res.* **2001**, *7*, 3574−3579.

(22) Merlot, A. M.; Kalinowski, D. S.; Richardson, D.R.; *Antioxid. Redox. Signal.* **2013**, *18*, 973−1006.

(23) Zhu, L.; Zhou, B.; Chen, W.; Jiang, H.; Shao, J.; Yen, Y. *Biochem. Pharm.* **2009**, *78*, 1178−1185.

(24) Popović-Bijelić, A.; Kowol, C. R.; Lind, M. E.; Luo, J.; Himo, F.; Enyedy, E. A.; Arion, V. B.; Gräslund, A. *J. Inorg. Biochem.* **2011**, *105*, 1422−1431.

(25) Aye, Y.; Long, M. J. C.; Stubbe, J. *J. Biol. Chem.* **2012**, *287*, 35768−35778.

(26) Nitiss, J. L. *Nat. Rev. Cancer* **2009**, *9*, 327−337.

(27) Schoeffler, A. J.; Berger, J. M. *Q. Rev. Biophys*. **2008**, *41*, 41−101.

(28) Easmon, J.; Puerstinger, G.; Heinisch, G.; Roth, T.; Fiebig, H. H.; Holzer, W.; Jaeger, W.; Jenny, M.; Hofmann, J. *J. Med. Chem.* **2001**, *44*, 2164−2171.

(29) Wei, L.; Easmon, J.; Nagi, R. K.; Muegge, B. D.; Meyer, L. A.; Lewis, J. S. *J. Nucl. Med.* **2006**, *47*, 2034−2041.

(30) Huang, H.; Chen, Q.; Ku, X.; Meng, L.; Wang, X.; Zhu, C.; Wang, Y.; Chen, Z.; Li, M.; Jiang, H.; Chen, K.; Ding, J.; Liu, H. *J. Med. Chem.* **2010**, *53*, 3048−3064.

(31) Zeglis, B. M.; Divilov, V.; Lewis, J. S. *J. Med. Chem.* **2011**, *54*, 2391−2398.

(32) Prabhakaran, R.; Kalaivoni, P.; Huang, R.; Poornima, P.; Padma, V. V.; Dallemer, F.; Natarajan, K. *J. Biol. Inorg. Chem.* **2013**, *18*, 233−247.

(33) Pahontu, E.; Fala, V.; Gulea, A.; Poier, D.; Tapcov, V.; Rosu, T. *Molecules* **2013**, *18*, 8812−8836.

(34) Datta, S.; Seth, D. K.; Gangopadhyay, S.; Karmakar, P.; Bhattacharya, S. *Inorg. Chim. Acta* **2012**, *392*, 118−130.

(35) Ramchandran, E.; Raja, D. S.; Bhuvanesh, N. S. P.; Natarajan, K. *Eur. J. Med. Chem.* **2013**, *64*, 179−189.

(36) Ramchandran, E.; Raja, D. S.; Mike, J. L.; Wagner, T. R.; Zeller, M.; Natarajan, K. *RSC Adv*. **2012**, *2*, 8515−8525.

(37) Basu, A.; Thiyagarajan, D.; Kar, C.; Ramesh, A.; Das, G. *RSC Adv.* **2013**, *3*, 14088−14098

(38) Helm, L.; Merbach, A. E. *J. Chem. Soc. Dalton Trans.* **2002**, 633−641.

(39) Prabhakaran, R.; Kalaivani, P.; Poorima, P.; Dallemer, F.; Paramaguru, G.; Padma, V. V.; Renganathan, R.; Huang, R.; Natarajan, K. *Dalton Trans.* **2012**, *41*, 9323−9336.

(40) Palanimunthu, D.; Samuelson, A. G. *Inorg. Chim. Acta* **2013**, *408*, 152−161.

(41) Yousef, T. A.; El-Reash, G. M. A.; Al-Jahdali, M.; El-Rakhawy, E.-B. R. *Spectrochim. Acta A* **2014**, 163−172.

(42) Tan, K. W.; Seng, H. L.; Lim, F. S.; Cheah, S.-C; Ng, C. H.; Koo, K. S.; Mustafa, M. R.; Ng, S. W.; Maah, M. J. *Polyhedron* **2012**, *38*, 275−284.

(43) Knight, J. M.; Whelan, H.; Petering, D. H. *J. Inorg. Biochem.* **1979**, *11*, 327−338.

(44) Milunovic, M. N. M.; Enyedy, E. A.; Nagy, N. V.; Kiss, T.; Trondl, R.; Jakupec, M. A.; Keppler, B. K.; Krachler, R.; Novitchi, G.; Arion, V. B. *Inorg. Chem.* **2012**, *51*, 9309−9321.

(45) Enyedy, É. A.; Zsigó, É.; Nagy, N. V.; Kowol, C. R.; Roller, A.; Keppler, B. K.; Kiss, T. *Eur. J. Inorg. Chem.* **2012**, 4036−4047.

(46) Enyedy, É. A.; Primik, M. F.; Kowol, C. R.; Arion, V. B.; Kiss, T.; Keppler, B. K. *Dalton Trans.* **2011**, *40*, 5895−5905.

(47) (a) Enyedy, É. A.; Nagy, N. V.; Zsigó, É.; Kowol, C. R.; Arion, V. B.; Keppler, B. K.; Kiss, T. *Eur. J. Inorg. Chem.* **2010**, 1717−1728; (b) Enyedy, É. A.; Bognár, G. M.; Nagy, N. V.; Jakusch, T.; Kiss, T.; Gambino, D. *Polyhedron* **2014**, *67*, 242−252.

(48) Li, Y.; De Kock, C.; Smith, P. J.; Chiballe, K.; Smith, G. S. *Organometallics* **2014**, *33*, 4345−4348.

(49) Bacher, F.; Enyedy, É. A.; Nagy, N. V.; Rockenbauer, A.; Bognár, G. M.; Trondl, R.; Novak, M. S.; Klapproth, E.; Kiss, T.; Arion, V. B. *Inorg. Chem.* **2013**, *52*, 8895−8908.

(50) Kowol, C. R.; Berger, R.; Eichinger, R.; Roller, A.; Jakupec, M. A.; Schmidt, P. P.; Arion, V. B.; Keppler, B. K. *J. Med. Chem.* **2007**, *50*, 1254−1265.

(51) Kowol, C. R.; Eichinger, R.; Jakupec, M. A.; Galanski, M.; Arion, V. B.; Keppler, B. K. *J. Inorg. Biochem.* **2007**, *101*, 1946−1957.

(52) Arion, V. B.; Jakupec, M. A.; Galanski, M.; Unfried, P.; Keppler, B. K. J. *Inorg. Biochem.* **2002**, *91*, 298−305.

(53) Enyedy, É. A.; Primik, M. F.; Kowol, C. R.; Arion, V. B.; Kiss, T.; Keppler, B. K. *Dalton Trans.* **2011**, *40*, 5895−5905.

(54) Kowol, C. R.; Trondl, R.; Heffeter, P.; Arion, V. B.; Jakupec, M. A.; Roller, A.; Galanski, M.; Berger, W.; Keppler, B. K. *J. Med. Chem.* **2009**, *52*, 5032−5034.

(55) Williams, D. B. G.; Lawton, M. *J. Org. Chem.* **2010**, *75*, 8351–8354.

(56) Paolucci, G.; Zanella, A.; Bortoluzzi, M.; Sostero, S.; Longo, P.; Napoli, M. *J. Mol. Catal.* **2007**, *272*, 258–264.

(57) Gans, P.; Sabatini, A.; Vacca, A. *Talanta* **1996**, *43*, 1739–1753.

(58) Irving, H. M.; Miles, M. G.; Pettit, L. D. *Anal. Chim. Acta* **1967**, *38*, 475–488.

(59) SCQuery, The IUPAC Stability Constants Database, Academic Software (Version 5.5).

(60) Zékány, L.; Nagypál, I. in: *Computational Methods for the Determination of Stability Constants* (Ed.: D. L. Leggett), Plenum Press, New York, **1985**, p. 291–353.

(61) *SAINT-Plus*, version 7.06a and APEX2; Bruker-Nonius AXS Inc.: Madison, WI, 2004;

(62) Sheldrick, G. M. *Acta Crystallogr. A* **2008**, *64*, 112−122.

(63) Farrugia, L. J. *J. Appl. Crystallogr.* **1997**, *30*, 565.

(64) Bencini, A.; Gatteschi, D. In *EPR of Exchange Coupled Systems*; Springer Verlag: Berlin-Heidelberg, 1990.

(65) Joung, K. O.; O'Connor, C. J.; Sinn, E.; Carlin, R. L. *Inorg. Chem.* **1979**, *18*, 804−808.

(66) Sakiyama, H.; Suzuki, T.; Ono, K.; Ito, R.; Watanabe, Y.; Yamasaki, M.; Mikuriya, M. *Inorg. Chim. Acta* **2005**, *358*, 1897−1903.

(67) Kopel, P.; Trávniček, Z.; Marek, J. R.; Mrozinski, J. *Polyhedron* **2004**, *23*, 1573−1578.

(68) Carlin, R.; Van Duyneveldt, A. *Magnetic Properties of Transition Metal Compounds.* Springer-Verlag, New York, 1977.

(69) Hassan, A. K.; Pardi, L. A.; Krzystek, J.; Sienkiewicz, A.; Goy, P.; Rohrer, M.; Brunel, L.-C. *J. Magn. Reson*. **2000**, 142, 300−312.

(70) (a) Tran, B. L.; Krzystek, J.; Ozarowski, A.; Chen, C. H.; Pink, M.; Karty, J. A.; Telser, J.; Meyer, K.; Mindiola, D. J. *Eur. J. Inorg. Chem.*, **2013**, 3916–3929; (b) Semenaka, V. V.; Nesterova, O. V.; Kokozay, V. N.; Dyakonenko, V. V.; Zubatyuk, R. I.; Shishkin, O. V.; Boča, R.; Jezierska, J.; Ozarowski, A. *Inorg. Chem.* **2010**, *49*, 5460–5471; (c) Herchel, R.; Boča, R.;

Krzystek, J.; Ozarowski, A.; Duran, M.; van Slageren, J. *J. Am. Chem. Soc.* **2007***, 129*, 10306–10307.

(71) Supino, R. *In Vitro Toxicity Testing Protocols*, **1995**, 137–149.

(72) Pessôa, M. M. B.; Andrade, G. F. S.; Monteiro, V. R. P.; Temperine, M. L. A. *Polyhedron* **2001**, *20*, 3133–3141.

(73) Addison, A. W.; Rao, T. N.; Reedijk, J.; van Rijn, J.; Verschoor, G. C. *J. Chem. Soc. Dalton Trans.* **1984**, 1349–1356.

(74) Lobana, T. S.; Kumari, P.; Castineiras, A.; Butcher, R. J. *Eur. J. Inorg. Chem.* **2013**, 3557–3566.

(75) a) Sunkel, K.; Hoffmuller, W.; Beck, W. *Z. Naturforsch.* **1998**, *53b*, 1365–1368; b) Poth, T.; Paulus, H.; Elias, H.; Dücker-Benfer, C.; van Eldik, R. *Eur. J. Inorg. Chem.* **2001**, 1361–1369; c) Yousef, R. I.; Bette, M.; Kaluderović, G. N.; Paschke, R.; Yiran, C.; Steinborn, D.; Schmidt, H. *Polyhedron* **2011**, *30*, 1990–1996; d) Carmona, D.; Lahoz, F. J.; Atencio, R.; Oro, L. A.; Lamata, M. P.; Viguri, F.; José, E. S.; Vega, C.; Reyes, J.; Joó, F.; Kathó, Á. *Chem. Eur. J.* **1999**, *5*, 1544–1564.

(76) Carmona, D.; Lamata, M. P.; Viguri, F.; Dobrinovich, I.; Lahoz, F. L.; Oro, L. A. *Adv. Synth. Catal.* **2002**, *344*, 499–502.

(77) (a) Neese, F. *J. Phys. Chem. Solids* **2004**, *65*, 781–785; (b) Maurice, R.; Sivalingam, K.; Ganyushin, D.; Guihery, N.; de Graaf, C.; Neese, F. *Inorg. Chem.* **2011**, *50*, 6229–6236; (c) Onofrio, N.; Mouesca, J.-M. *Inorg. Chem.* **2011**, *50*, 5577–5586; (d) Rodríguez-Fortea, A.; Alemany, P.; Alvarez, S.; Ruiz, E. *Inorg. Chem.* **2002**, *41*, 3769–3778.

(78) (a) Neese, F. *ORCA* - An ab initio, Density Functional and Semiempirical Program Package, Version 2.9.1, 2012. (b) Neese, F. WIREs *Comput. Mol. Sci.* **2012**, *2*, 73–78.

(79) (a) Schaefer, A.; Horn, H.; Ahlrichs, R. *J. Chem. Phys.* **1992**, *97*, 2571–2577; (b) Ahlrichs, R. *et al*., unpublished; (c) The Ahlrichs auxiliary basis sets were obtained from the TurboMole basis set library under ftp.chemie.uni-karlsruhe.de/pub/jbasen; (d) Eichkorn, K.; Treutler, O.; Ohm, H.; Haser, M.; Ahlrichs, R. *Chem. Phys. Lett.* **1995**, *240*, 283–290; (e) Eichkorn, K.; Weigend, F.; Treutler, O.; Ahlrichs, R. *Theor. Chem. Acc.* **1997**, *97*, 119–124.

(80) (a) Becke, D. A.; *Phys. Rev. A* **1988***, 38*, 3098−3100; (b) Perdew, J. P. *Phys. Rev. B* **1986***, 33,* 8822−8824; (c) Perdew, J. P. *Phys. Rev. B.* **1986***, 34*, 7406−7406; (d) Kendall, R. A.; Früchtl, H. A. *Theor. Chem. Acc.* **1997**, 97, 158−163.

(81) Reger, D. L.; Pascui, A. E.; Smith, M. D.; Jezierska, J.; Ozarowski, A. *Inorg. Chem.* **2012**, *51*, 11820−11836.

(82) Moriya, T. *Phys. Rev.* **1960**, *120*, 91−98.

(83) Masouka, J.; Saltman, P. *J. Biol. Chem.* **1994**, *269*, 25557–25561.

(84) Ohyoshi, E.; Hamada, Y.; Nakata, K.; Kohata, S. *J. Inorg. Biochem.* **1999**, *75*, 213–218.

(85) Harris, W. R. *Biochemistry* **1983**, *22*, 3920–3926.

(86) Bal, W.; Sokołowska, M.; Kurowska, E.; Faller, P. *Biochim. Biophys. Acta* **2013**, *1830*, 5444–5455.

(87) (a) Richardson, D. R.; Kalinowski, D. S.; Richardson, V.; Sharpe, P.; Lovejoy, D. B.; Islam, M.; Bernhardt, P. V. *J. Med. Chem.* **2009**, *52*, 1459−1470; (b) Easmon, J.; Heinisch, G.; Holzer, W.; Rosenwirth, B. *J. Med. Chem.* **1992**, *35*, 3288−3296.

(88) Kuhn, P.-S.; Büchel, G.; Jovanovic, K.; Filipovic, L.; Radulovic, S.; Rapta, P.; Arion, V. B. *Inorg. Chem.* **2014**, 53, 11130−11139.

(89) Ochiai, E.; Mann, G. J.; Gräslund, A.; Thelander, L. *J. Biol. Chem*. **1990**, *265*, 15758−15761.

(90) Heffeter, P.; Popović-Bijelić, A.; Saiko, T.; Dornetshuber, R.; Jungwirth, U.; Voevodskaya, N.; Biglino, D.; Jakupec, M.A.: Elbling, L.; Micksche, M.; Szekeres, T.; Keppler, B.K.; Gräslund, A.; Berger, W. *Curr. Cancer Drug Targets* **2009**, *9*, 595−607.

Table of Contents

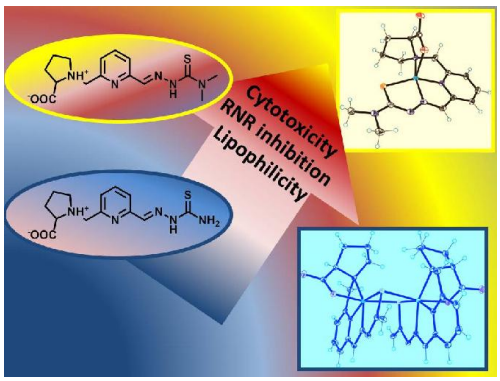

Terminal dimethylation and copper(II) coordination of proline – 2-formylpyridine thiosemicarbazone hybrids resulted in enhanced lipophilicity, antiproliferative activity in human cancer cell lines and enhanced hR2 RNR inhibition.